SAND80-0085
Unlimited Release

VAWTDYN - A NUMERICAL PACKAGE FOR THE DYNAMIC ANALYSIS OF VERTICAL AXIS WIND TURBINES

D. W. Lobitz and W. N. Sullivan

Prepared by Sandia Laboratories, Albuquerque, New Mexico 87185 and Livermore, California 94550 for the United States Department of Energy under Contract AT(29-1)-789

Printed July 1980

When printing a copy of any digitized SAND Report, you are required to update the markings to current standards.

Sandia Laboratories
energy report

Issued by Sandia Laboratories, operated for the United States Department of Energy by Sandia Corporation.

NOTICE

This report was prepared as an account of work sponsored by the United States Government. Neither the United States nor the Department of Energy, nor any of their employees, nor any of their contractors, subcontractors, or their employees, makes any warranty, express or implied, or assumes any legal liability or responsibility for the accuracy, completeness or usefulness of any information, apparatus, product or process disclosed, or represents that its use would not infringe privately owned rights.

SF 1004-DF(11-77)

SAND80-0085
Unlimited Release

VAWTDYN - A NUMERICAL PACKAGE FOR THE DYNAMIC ANALYSIS OF VERTICAL AXIS WIND TURBINES

D. W. Lobitz
Applied Mechanics Division I
Division 5521

W. N. Sullivan
Advanced Energy Projects
Division 4715

Sandia National Laboratories
Albuquerque, New Mexico 87185

Abstract

In order to design wind turbines which possess long life and at the same time use a minimum quantity of low-cost materials, it is essential that dynamic, in addition to static, structural analyses be performed to eliminate unnecessary margins of safety resulting from undetermined dynamic amplifications. The VAWTDYN package provides a tool for assessing these amplifications in two-bladed vertical axis wind turbines. The dynamic model on which the package is based contains turbine motions most commonly observed in existing research systems. Gyroscopic effects, structural damping, aerodynamic wind loading, and power generation through either an induction or synchronous generator are also included in the model. In addition to a comprehensive description of the model, this report documents the efforts that have gone into the verification, qualification, and demonstration of the package.

Acknowledgement

The authors gratefully acknowledge the efforts of T. M. Leonard (UNM/New Mexico Engineering Research Institute) in assisting in the preparation of this package. In addition to general computer programming assistance, Mr. Leonard is solely responsible for the powerful plotting package which has proven to be invaluable in post-processing VAWTDYN output.

VAWTDYN - A NUMERICAL PACKAGE FOR THE DYNAMIC ANALYSIS OF VERTICAL AXIS WIND TURBINES

I Introduction

The Darrieus vertical axis wind turbine (VAWT) has been investigated for the past several years as a potentially valuable alternate energy producer. The future utility of the VAWT (and of virtually all other wind-powered energy-producing schemes) depends to a large degree on developing the ability to design rotors with long structural life using the minimum quantity of low-cost materials. In the structural design of a VAWT rotor, dynamic effects are important because they govern the fatigue life of the rotor. The major source of dynamic effects is aerodynamic loading[1] which varies substantially and periodically as the rotor turns relative to the ambient wind direction.

The design of early generation operational VAWT rotors (Fig. 1) has relied primarily on quasi-static finite element analyses for rotor design[2]. In this technique, peak values of the time-varying aerodynamic loads are applied to the rotor statically. The resulting stress predictions can be accurate[3] if the resonant frequencies of the rotor are well above the dominant excitation frequencies in the aerodynamic load functions. However, because this is not necessarily the case for all load conditions, early VAWT rotors were designed with substantial factors of safety to account for possible dynamic stress amplification in the rotor.

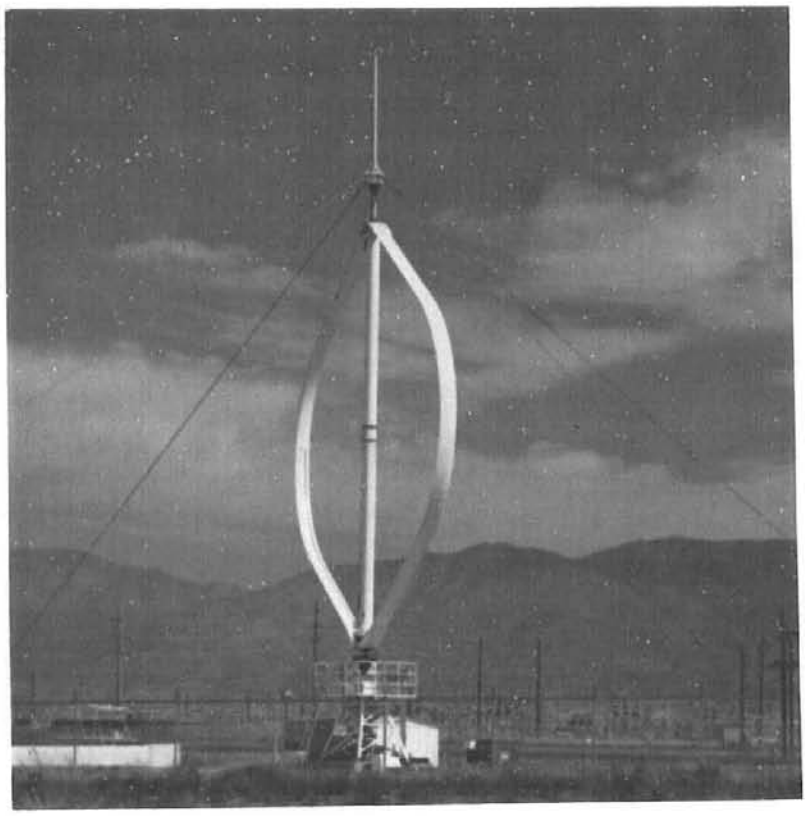

Figure 1: The DOE/Sandia 17 Meter Vertical Axis Wind Turbine

In the interest of reducing costs and increasing reliability of future generation rotors, more complete and reliable approaches to dynamic modeling need to be incorporated in the design process. This is the motivation for the development of the VAWTDYN package.

Prior to the development of VAWTDYN, consideration was given to adapting previously developed rotating wind dynamics packages to analyze the VAWT. Although many of these packages are of a proprietary nature, some are available for purchase. For example, MOSTAB-HFW[4], an adaptation of MOSTAS developed for helicopter rotor analysis, has been used with some success in

the analysis of DOE/NASA's horizontal axis wind turbine (HAWT) rotors. After discussions with appropriate NASA personnel as to the possibility of adopting HAWT-developed software for the dynamic analysis of VAWT's, it was determined that the necessary modifications to MOSTAS or a similar helicopter-type software package would be more extensive than developing a new package expressly for the VAWT. Consideration was also given to adapting packages[5,6] developed for studying VAWT dynamic stability to address the general problem of dynamic response. However, this was not pursued because of the relative inaccessibility and complexity of these methods.

An attempt was made in the development of VAWTDYN to begin with a relatively simple representation of the rotor to permit development of intuition in identifying the important dynamic effects. As a result, in its current form, VAWTDYN is usable only for two-bladed rotors with motions limited to those most commonly observed in research systems. The model can conceivably be expanded, at the expense of complexity, if experimental data indicate that more complete representation is appropriate. Since a capability to analyze forced vibrations was desired, VAWTDYN includes aerodynamic wind loadings. Provisions were also made for the inclusion of structural damping and for the connection of the turbine to either a synchronous or an induction generator. Of course, the model contains all appropriate gyroscopic effects.

This report is intended primarily to serve as a description of the model from which the software was developed. There have been limited comparisons of VAWTDYN predictions to certain measured data on the DOE/Sandia 17-m research turbine (Fig. 1.) These comparisons have been very encouraging and, consequently, it is felt that the package can potentially be used in the design process. However, further refinement and confirmation are advisable prior to using the program on a production basis. Follow-up reports are planned as data and experience with the package accumulate.

The remainder of the report contains results of computations performed for the verification and qualification of the software package, and presents examples which demonstrate the usefulness of the package.

Description of the Model

The basic model consists of a number of rigid bodies interconnected by a network of springs, dashpots, and joints. The point on the tower at the lower blade attachment is fixed in space. Although the structure can rotate about this point, no translations are permitted. The origin of a rotating coordinate system (the xyz system) employed in the model is placed at this point. With the z axis always passing through the blade upper attachment point on the tower, the rotating

system is constrained to rotate with the tower. Referring to Fig. 2, the rotating coordinate system has three degrees of

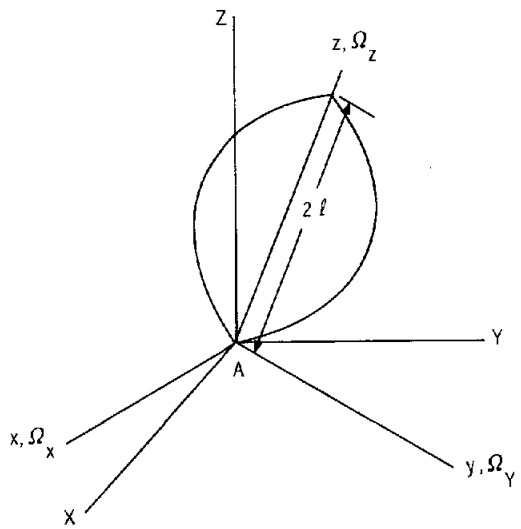

Figure 2: Description of the Rotating Coordinate System Employed by the Model

freedom, Ω_x, Ω_y and Ω_z, associated with its angular velocity relative to the stationary XYZ system.

Within this rotating frame, tower motions are allowed which represent deformation patterns of the tower in a first-mode response. As shown in Fig. 3, the model of the tower is composed of two rigid links of equal length, joined together with a "U" joint. Thus, the joint is capable of transmitting lateral and axial forces as well as a moment in the z direction. Note again that the z axis always passes through the lowest and uppermost points of the tower. The midpoint of the tower can experience u and v displacements, as shown.

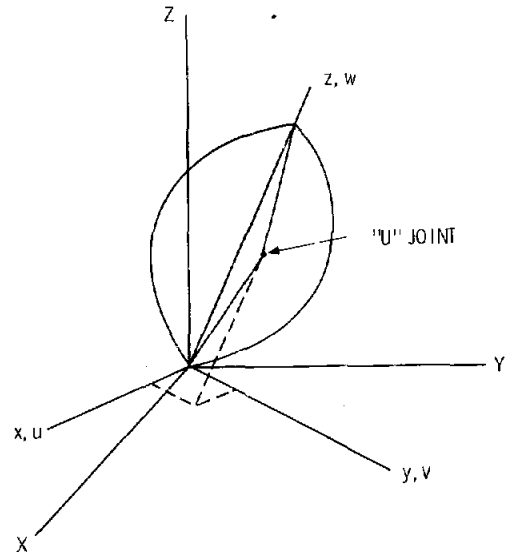

Figure 3. Tower Motions Within the Rotating Frame Permitted by the Model

Through kinematics the w displacement can be determined in terms of u and v. To represent the tower stiffness and damping, torsional springs and dashpots, which develop restoring moments in the x and y directions, are attached in parallel at the "U" joint. The associated spring and damping constants, K_x, K_y, C_x, and C_y, for restoring moments about the x and y axes, respectively, are input quantities. The x and y quantities are not necessarily equal if one wishes to consider the effect of the bending stiffness of the blades in the tower motions.

The tower is connected to the transmission via a torsional spring, K_B, and parallel dashpot, C_B, through which the turbine drives the generator. The generator can be either synchronous, in which case the angular velocity history of the

rotor is prescribed, or induction, where the torque on the rotor is given as a function of rotor RPM.

The guy cables at the top of the tower are represented by a spring, K_G, associated with the stiffness perpendicular to the z axis of the rotating system, and a vertical force, G_z, down the z axis. At present, the guy cables are assumed to behave linearly but can be made nonlinear to take into account such effects as cable droop. A dashpot, C_G, is connected in parallel with the spring to account for the damping in the cables.

Each of the two turbine blades is modeled as a rigid body attached to the tower through two ball joints which can transmit force in the x and y directions. As shown in Fig. 4,

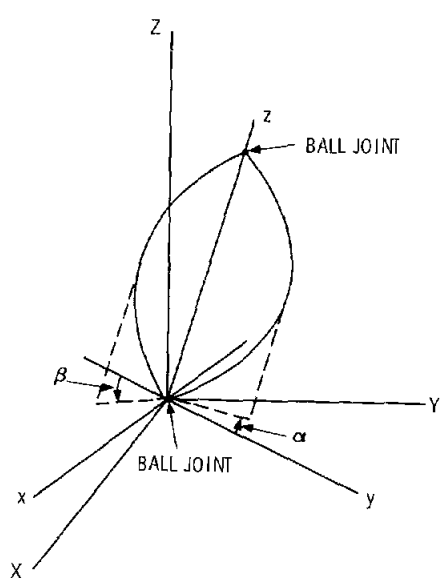

Figure 4: Blade Motions Within the Rotating Frame Permitted by the Model

the blades can move independently of each other about the z axis, in and out of the yz plane, through angles of α and β, respectively. The lead-lag stiffness and damping of each blade is modeled with a torsional spring, K_T, and dashpot, C_T, which develop moments about the z axis at each ball joint, tending to restore the blade to its equilibrium position in the yz plane. Since the blade moves as a rigid body, no motion perpendicular to the chord of the blade in the rotating coordinate system is permitted.

The motions described above for this discrete model are clearly a subset of those possible for the wind turbine. However, this subset includes all the predominant motions that have been observed in Sandia's VAWT's. Future efforts may involve expanding the subset.

Although a number of approaches are available for the development of the equations of motion, the more direct approach of simply using Newton's 2nd Law of motion was selected. The equations of motion for each rigid segment of the turbine (i.e., the blades, tower segments, etc) were derived, carefully including the unknown interconnecting forces. In cases where a segment of the model is attached to the point on the tower at the lower blade connection, which is fixed in space, it is necessary to consider only the rate of change of the moment of

momentum in developing the equations of motion. Otherwise, the rates of change of both the moment of momentum and linear momentum must be taken into account.

As an example of the method used, the equations of motion for one of the blades are developed below. In this case, only the rate of change of the moment of momentum about the blade-tower lower attachment point need be considered. If this point is denoted as point A then H_A is the angular momentum vector of the blade about point A. The time rate of change of the angular momentum, which is of course equal to the sum of the applied moments about point A, is given by

$$\left(\frac{d\underset{\sim}{H}_A}{dt}\right)_{XYZ} = \left(\frac{d\underset{\sim}{H}_A}{dt}\right)_{xyz} + \underset{\sim}{\Omega} \times \underset{\sim}{H}_A \quad . \tag{1}$$

Here the subscripts XYZ and xyz denote the time derivative relative to the fixed XYZ and rotating xyz coordinate systems, respectively. The vector, $\underset{\sim}{\Omega}$, is the unknown angular velocity vector of the rotating system. Referring to the right hand blade in Fig. 4, the angular velocity vector of the blade, $\underset{\sim}{\omega}$, is given by

$$\underset{\sim}{\omega} = \begin{Bmatrix} \Omega_x \\ \Omega_y \\ \Omega_z + \dot{\alpha} \end{Bmatrix} \quad . \tag{2}$$

In the case where $\alpha = 0$, the inertia tensor of the blade is given by

$$\underset{\approx}{I}(\alpha=0) = \begin{bmatrix} I_{xx} & 0 & 0 \\ 0 & I_{yy} & -I_{yz} \\ 0 & -I_{yz} & I_{zz} \end{bmatrix} .$$

Using the transformation,

$$\underset{\approx}{a} = \begin{bmatrix} \cos\alpha & \sin\alpha & 0 \\ -\sin\alpha & \cos\alpha & 0 \\ 0 & 0 & 1 \end{bmatrix} ,$$

the expression for $I(\alpha)$ given below is obtained:

$$\underset{\approx}{I}(\alpha) = \underset{\approx}{a}\, \underset{\approx}{I}(\alpha=0)\, \underset{\approx}{a}^{T} \quad . \tag{3}$$

The angular momentum vector then is given by

$$\underset{\sim}{H}_A = \underset{\approx}{I}(\alpha)\, \underset{\sim}{\omega} \quad . \tag{4}$$

With this expression, Eq. (1) becomes

$$\left(\frac{d\underset{\sim}{H}_A}{dt}\right)_{XYZ} = \left[\frac{d\underset{\approx}{I}(\alpha)}{dt}\right]_{xyz} \underset{\sim}{\omega} + \underset{\approx}{I}(\alpha)\left(\frac{d\underset{\sim}{\omega}}{dt}\right)_{xyz} + \Omega \times [\underset{\approx}{I}(\alpha)\underset{\sim}{\omega}] \quad . \tag{5}$$

Due to algebraic complexity, the expansion of the above equation is presented in Appendix A.

A number of terms in this equation can be eliminated by considering the motions of the turbine, aside from the general rotation, to be small. In fact, if the ratio of the maximum deflection, δ, at the top of the tower to the tower length, 2ℓ, is limited to .01 (this corresponds to a deflection of approximately 6 in. on Sandia's 17 meter turbine), Ω_x and Ω_y can be shown to be small compared to Ω_z. Using the fact that the highest excitation frequencies are generally less than 10 times the operating frequency, the following approximations can be made:

$$\Omega_x \ , \ \Omega_y = O(10\Omega_z \frac{\delta}{2\ell}) = O(.1\Omega_z)$$

$$\dot{\Omega}_x \ , \ \dot{\Omega}_y = O(10^2\Omega_z^2 \frac{\delta}{2\ell}) = O(\Omega_z^2) \quad .$$

Additionally, if the ratio of the lead-lag deflection at the outermost extremity of the blade, to the turbine radius is limited to .01 (this corresponds to a deflection of

approximately 3 in. on Sandia's 17 meter turbine), α must also be limited to this value, and the approximations $\sin\alpha \approx \alpha$ and $\cos\alpha \approx 1$ can be made. Using a rationale similar to that for Ω_x and Ω_y, it can be shown that for $\alpha \leq .01$, $\dot{\alpha} = 0(.1\Omega_z)$ and $\ddot{\alpha} = 0\left(\Omega_z^2\right)$. Finally, it is assumed that $\dot{\Omega}_z = 0(\ddot{\alpha}) = 0\left(\Omega_z^2\right)$.

Using the above order of magnitude estimates to eliminate higher order terms, Eq. (5), which has been expanded in Appendix A, reduces to

$$\left(\frac{d\underset{\sim}{H}_A}{dt}\right)_{XYZ} = \begin{Bmatrix} -I_{yz}\dot{\alpha}\Omega_z + I_{xx}\dot{\Omega}_x + (I_{zz} - I_{yy})\,\Omega_y\Omega_z + I_{yz}\Omega_z^2 \\ I_{yy}\dot{\Omega}_y - I_{yz}(\dot{\Omega}_z + \ddot{\alpha}) + (I_{xx} - I_{zz})\,\Omega_x\Omega_z \\ -I_{yz}\dot{\Omega}_y + I_{zz}(\dot{\Omega}_z + \ddot{\alpha}) - I_{yz}\Omega_x\Omega_z \end{Bmatrix} \tag{6}$$

Now that the time-rate of change of angular momentum has been established, the external moments about the lower blade-tower attachment point need to be determined and cast in terms of the rotating coordinate system. Moments due to the wind loading of the blade, the interconnecting forces, and the torsional springs and dashpots mounted between the tower and the blades need to be considered. Referring to Fig. 5, the total moment, $\underset{\sim}{M}_A$, acting on the blade about point A is given by

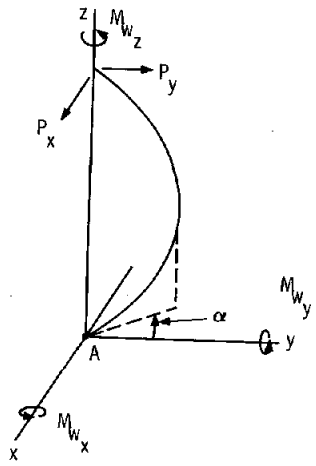

Figure 5: Blade Loadings Which Produce Moments About the Lower Attachment Point, "A"

$$\underset{\sim}{M}_A = \begin{Bmatrix} M_{w_x} - 2\ell P_y \\ M_{w_y} + 2\ell P_x \\ M_{w_z} - 2K_T\alpha - 2\,C_T\,\dot{\alpha} \end{Bmatrix} . \tag{7}$$

Here, ℓ is one-half the length of the tower. The quantities, M_{w_x}, M_{w_y}, and M_{w_z}, are the moments due to aerodynamic loads and will be discussed in greater detail below. Note that the moment due to gravity has been neglected. Setting Eq. (6) equal to Eq. (7) yields the equations of motion for the blade.

Before doing this, however, one final modification is desirable. To illuminate the "propeller" (blade motion in phase) and "butterfly" (blade motion out of phase) behavior of

the composite blade motion, the variables, α and β, have been replaced by η and ρ, defined as shown:

$$\eta = \alpha + \beta \quad , \quad \rho = \alpha - \beta \quad .$$

Then, in terms of η and ρ,

$$\alpha = \frac{\eta + \rho}{2} \quad , \quad \beta = \frac{\eta - \rho}{2} \quad .$$

With this change, the final equations of motion for the blade are given by

$$\begin{Bmatrix} -I_{yz} \frac{\dot{\eta} + \dot{\rho}}{2} \Omega_z + I_{xx}\dot{\Omega}_x + (I_{zz} - I_{yy}) \Omega_y \Omega_z + I_{yz}\Omega_z^2 \\ I_{yy}\dot{\Omega}_y - I_{yz}\left(\dot{\Omega}_z - \frac{\ddot{\eta} + \ddot{\rho}}{2}\right) + (I_{xx} - I_{zz}) \Omega_x \Omega_z \\ -I_{yz}\dot{\Omega}_y + I_{zz}\left(\dot{\Omega}_z + \frac{\ddot{\eta} + \ddot{\rho}}{2}\right) - I_{yz}\Omega_x \Omega_z \end{Bmatrix}$$

$$= \begin{Bmatrix} M_{w_x} - 2\ell P_y \\ M_{w_y} + 2\ell P_x \\ M_{w_z} - 2K_T \frac{\eta + \rho}{2} - 2C_T \frac{\dot{\eta} + \dot{\rho}}{2} \end{Bmatrix} . \tag{8}$$

In developing the equations of motion for the remaining components of the turbine, the angular position as a function of

time of the tower relative to the ground is required to determine the magnitude and direction of the forces developed by the tiedown cables. This angular position is obtained in in terms of the Euler angles defined in Fig. 6. The relation-

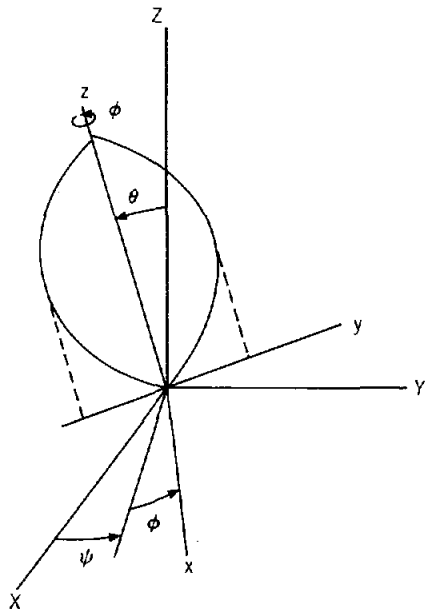

Figure 6: Description of the Euler Angles Employed by the Model

ship between these angles and $\dot{\underset{\sim}{\Omega}}$ is given below:

$$\dot{\underset{\sim}{\Omega}} = \begin{Bmatrix} (\ddot{\Psi}\sin\theta + \dot{\Psi}\dot{\theta}\cos\theta - \dot{\theta}\dot{\varphi})\sin\varphi + (\ddot{\theta} + \dot{\Psi}\dot{\varphi}\sin\theta)\cos\varphi \\ (-\ddot{\theta} - \dot{\Psi}\dot{\theta}\sin\theta)\sin\varphi + (\ddot{\Psi}\sin\theta + \dot{\Psi}\dot{\theta}\cos\theta - \dot{\theta}\dot{\varphi})\cos\varphi \\ \ddot{\varphi} + \ddot{\Psi}\cos\theta - \dot{\Psi}\dot{\theta}\sin\theta \end{Bmatrix} . \tag{9}$$

Normally with Euler angles, the vertical configuration corresponds to $\theta = 0°$. However, in the case of wind turbine, this choice leads to ill conditioning in the numerical integration procedure because, even though the motion of the turbine remains well behaved, ψ and ϕ mathematically go through relatively large changes in small time intervals as θ nears 0° (i.e., a vertical position of the tower). This difficulty can be avoided by choosing $\theta = 90°$ to correspond to the vertical position. In this way, both ψ and $\theta - \pi/2$ remain small, and ϕ essentially equal to the angular rotation of the turbine. Experience has shown the latter choice to be far superior for speed and accuracy in the numerical integration of the equations of motion. For this choice, the forces, $\underset{\sim}{G}$, exerted by the guy wires on the tower, cast in the rotating coordinate system, are given by

$$
\begin{aligned}
G_x &= 2\ell K_G[(\theta - \pi/2)\sin\varphi - \Psi\cos\varphi] \\
&\quad + 2\ell C_G[\dot{\theta}\sin\varphi - \dot{\Psi}\cos\varphi] , \\
G_y &= 2\ell K_G[(\theta - \pi/2)\cos\varphi + \Psi\sin\varphi] \\
&\quad + 2\ell C_G[\dot{\theta}\cos\varphi + \dot{\Psi}\sin\varphi] , \\
G_z &= \text{const.}
\end{aligned}
\tag{10}
$$

In the above, the quantities $\theta - \pi/2$ and ψ are assumed to be small, consistent with the prior approximation that $\delta/2\ell \leq .01$.

The equations of motion for the complete model, coupled to a synchronous generator, are given in matrix form in Table 1. The first three equations are for the rotational motion of the lower rigid tower link about the base of the turbine. The next six describe the rotational motion and the translational motion of the center of mass of the upper rigid tower link, respectively, three equations for each. The next set of six define the rotational motion of each of the blades about the base of the turbine. And the final three give the relationship between the three angular accelerations, Ω_x, Ω_y, and Ω_z, and the Euler angles ψ (angle of precession), θ (angle of nutation), and ϕ (angle of spin). The nomenclature in these equations is defined as follows:

F_x, F_y, F_z, M_z	Interconnecting forces and moments between the upper and lower rigid tower links.
G_x, G_y, G_z	Forces exerted by the guy wires on the tower.
$M_{W_x}(\phi)$, $M_{W_x}(\phi+\pi)$ $M_{W_y}(\phi)$, $M_{W_y}(\phi+\pi)$ $M_{W_z}(\phi)$, $M_{W_z}(\phi+\pi)$	Resultant moments on the blades due to wind loading as a function of the angular rotation of the turbine.

Table 1: Equations of Motion for the Complete Two-Bladed Model.

$$
\begin{bmatrix}
\frac{m\ell^2}{3} & 0 & 0 & 0 & -\frac{m\ell^2}{3} & 0 & 0 & 0 & \ell & -v & 0 & 0 & 0 & 0 & 0 & 0 & 0 & 0 \\
0 & \frac{m\ell^2}{3} & 0 & \frac{m\ell^2}{3} & 0 & 0 & 0 & -\ell & 0 & u & 0 & 0 & 0 & 0 & 0 & 0 & 0 & 0 \\
0 & 0 & MR^2 & 0 & 0 & 0 & 0 & v & -u & 0 & -1 & 0 & 0 & 0 & 0 & 0 & 0 & 0 \\
\frac{m\ell^2}{12} & 0 & 0 & 0 & \frac{m\ell^2}{12} & 0 & 0 & 0 & \frac{\ell}{2} & \frac{v}{2} & 0 & 0 & -\frac{\ell}{2} & 0 & -\frac{\ell}{2} & 0 & 0 & 0 \\
0 & \frac{m\ell^2}{12} & 0 & -\frac{m\ell^2}{12} & 0 & 0 & 0 & -\frac{\ell}{2} & 0 & -\frac{u}{2} & 0 & \frac{\ell}{2} & 0 & \frac{\ell}{2} & 0 & 0 & 0 & 0 \\
0 & 0 & MR^2 & 0 & 0 & 0 & 0 & -\frac{v}{2} & \frac{u}{2} & 0 & 1 & \frac{v}{2} & -\frac{u}{2} & \frac{u}{2} & -\frac{u}{2} & 0 & 0 & 0 \\
0 & \frac{3m\ell}{2} & 0 & \frac{m\ell}{2} & 0 & 0 & 0 & 1 & 0 & 0 & 0 & 1 & 0 & 1 & 0 & 0 & 0 & 0 \\
-\frac{3m\ell}{2} & 0 & 0 & 0 & \frac{m\ell}{2} & 0 & 0 & 0 & 1 & 0 & 0 & 0 & 1 & 0 & 1 & 0 & 0 & 0 \\
\frac{mv}{2} & -\frac{mu}{2} & 0 & -\frac{3mu}{2} & -\frac{3mv}{2} & 0 & 0 & 0 & 0 & 1 & 0 & 0 & 0 & 0 & 0 & 0 & 0 & 0 \\
I_{xx} & 0 & 0 & 0 & 0 & 0 & 0 & 0 & 0 & 0 & 0 & 0 & 2\ell & 0 & 0 & 0 & 0 & 0 \\
0 & I_{yy} & -I_{yz} & 0 & 0 & \frac{-I_{yz}}{2} & \frac{-I_{yz}}{2} & 0 & 0 & 0 & 0 & -2\ell & 0 & 0 & 0 & 0 & 0 & 0 \\
0 & -I_{yz} & I_{zz} & 0 & 0 & \frac{I_{zz}}{2} & \frac{I_{zz}}{2} & 0 & 0 & 0 & 0 & 0 & 0 & 0 & 0 & 0 & 0 & 0 \\
I_{xx} & 0 & 0 & 0 & 0 & 0 & 0 & 0 & 0 & 0 & 0 & 0 & 0 & 0 & 2\ell & 0 & 0 & 0 \\
0 & I_{yy} & I_{yz} & 0 & 0 & \frac{I_{yz}}{2} & \frac{-I_{yz}}{2} & 0 & 0 & 0 & 0 & 0 & 0 & -2\ell & 0 & 0 & 0 & 0 \\
0 & I_{yz} & I_{zz} & 0 & 0 & \frac{I_{zz}}{2} & \frac{-I_{zz}}{2} & 0 & 0 & 0 & 0 & 0 & 0 & 0 & 0 & 0 & 0 & 0 \\
1 & 0 & 0 & 0 & 0 & 0 & 0 & 0 & 0 & 0 & 0 & 0 & 0 & 0 & 0 & 0 & -\sin\theta\sin\varphi & -\cos\varphi \\
0 & 1 & 0 & 0 & 0 & 0 & 0 & 0 & 0 & 0 & 0 & 0 & 0 & 0 & 0 & 0 & -\sin\theta\cos\varphi & \sin\varphi \\
0 & 0 & 1 & 0 & 0 & 0 & 0 & 0 & 0 & 0 & 0 & 0 & 0 & 0 & 0 & -1 & -\cos\theta & 0
\end{bmatrix}
\begin{bmatrix}
\dot{\Omega}_x \\ \dot{\Omega}_y \\ \dot{\Omega}_z \\ \frac{\ddot{u}}{\ell} \\ \frac{\ddot{v}}{\ell} \\ \ddot{\eta} \\ \ddot{p} \\ F_x \\ F_y \\ F_z \\ M_z \\ P_x \\ P_y \\ Q_x \\ Q_y \\ \ddot{\varphi} \\ \ddot{\psi} \\ \ddot{\theta}
\end{bmatrix}
= \text{RHS}
$$

Table 1: (Cont)

$$
\mathrm{RHS} = \begin{bmatrix}
2K_x \frac{v}{\ell} + 2C_x \frac{\dot{v}}{\ell} - \Omega_y\Omega_z\left(mR^2 - \frac{m\ell^2}{3}\right) + 2\,\Omega_z \frac{\dot{u}}{\ell}\frac{m\ell^2}{3} - \Omega_z^2 \frac{v}{\ell}\frac{m\ell^2}{3} \\
-2K_y \frac{u}{\ell} - 2C_y \frac{\dot{u}}{\ell} - \Omega_x\Omega_z\left(\frac{m\ell^2}{3} - mR^2\right) + 2\,\Omega_z \frac{\dot{v}}{\ell}\frac{m\ell^2}{3} + \Omega_z^2 \frac{u}{\ell}\frac{m\ell^2}{3} \\
K_T\eta + C_T\dot{\eta} - K_B(\varphi - \varphi_o) - C_B(\dot{\varphi} - \dot{\varphi}_o) \\
-2K_x \frac{v}{\ell} - 2C_x \frac{\dot{v}}{\ell} - \frac{\ell}{2} G_y - \frac{v}{2} G_z - \Omega_y\Omega_z\left(mR^2 - \frac{m\ell^2}{12}\right) - 2\Omega_z \frac{\dot{u}}{\ell}\frac{m\ell^2}{12} + \Omega_z^2 \frac{v}{\ell}\frac{m\ell^2}{12} \\
2K_y \frac{u}{\ell} + 2C_y \frac{\dot{u}}{\ell} + \frac{\ell}{2} G_x + \frac{u}{2} G_z - \Omega_x\Omega_z\left(\frac{m\ell^2}{12} - mR^2\right) - 2\Omega_z \frac{\dot{v}}{\ell}\frac{m\ell^2}{12} - \Omega_z^2 \frac{u}{\ell}\frac{m\ell^2}{12} \\
-\frac{u}{2} G_y + \frac{v}{2} G_x + K_T\eta + C_T\dot{\eta} \\
G_x - \Omega_x\Omega_z \frac{3m\ell}{2} + \Omega_z^2 \frac{u}{\ell}\frac{m\ell}{2} + \Omega_z \frac{\dot{v}}{\ell}\, m\ell \\
G_y - \Omega_y\Omega_z \frac{3m\ell}{2} + \Omega_z^2 \frac{v}{\ell}\frac{m\ell}{2} - \Omega_z \frac{\dot{u}}{\ell}\, m\ell \\
G_z - \Omega_x \frac{v}{\ell}\, m + \Omega_y \frac{\dot{u}}{\ell}\, m + (\Omega_x^2 + \Omega_y^2)\frac{3m\ell}{2} - \Omega_x\Omega_z \frac{u}{\ell}\frac{m\ell}{2} - \Omega_y\Omega_z \frac{v}{\ell}\frac{m\ell}{2} + \left[\left(\frac{\dot{u}}{\ell}\right)^2 + \left(\frac{\dot{v}}{\ell}\right)^2\right]\frac{3m\ell}{2} \\
-\Omega_z^2 I_{yz} - \Omega_y\Omega_z(I_{zz} - I_{yy}) + \tfrac{1}{2}(\dot{\eta} + \dot{\rho})\,\Omega_z I_{yz} + M_{w_x}(\varphi) \\
-\Omega_x\Omega_z(I_{xx} - I_{zz}) + \tfrac{1}{2}(\eta + \rho)\,\Omega_z^2 I_{yz} + M_{w_y}(\varphi) \\
-K_T(\eta + \rho) - C_T(\dot{\eta} + \dot{\rho}) + \Omega_x\Omega_z I_{yz} + M_{w_z}(\varphi) \\
\Omega_z^2 I_{yz} - \Omega_y\Omega_z(I_{zz} - I_{yy}) - \tfrac{1}{2}(\dot{\eta} - \dot{\rho})\,\Omega_z I_{yz} + M_{w_x}(\varphi + \pi) \\
-\Omega_x\Omega_z(I_{xx} - I_{zz}) - \tfrac{1}{2}(\eta - \rho)\,\Omega_z^2 I_{yz} + M_{w_y}(\varphi + \pi) \\
-K_T(\eta - \rho) - C_T(\dot{\eta} - \dot{\rho}) - \Omega_x\Omega_z I_{yz} + M_{w_z}(\varphi + \pi) \\
-\ddot{\theta}\varphi \sin\varphi + \ddot{\psi}\theta \cos\theta \sin\varphi + \ddot{\psi}\varphi \sin\theta \cos\varphi \\
-\ddot{\theta}\varphi \cos\varphi + \ddot{\psi}\theta \cos\theta \cos\varphi - \ddot{\psi}\varphi \sin\theta \sin\varphi \\
\ddot{\psi}\theta \sin\varphi
\end{bmatrix}
$$

P_x, P_y, Q_x, Q_y	Interconnecting forces between each blade and the top of the tower.
m, ℓ, R	The mass, length and radius of each rigid tower link.
I_{xx}, I_{yy}, I_{zz}, I_{yz}	The moments and products of inertia of the blade lying in its undeformed state in the first quadrant of the "yz" plane.
ϕ_o, $\dot{\phi}_o$	The angular position and velocity of the low speed transmission shaft below the tower torsional spring (K_B) and dashpot (C_B).
K_x, K_y, C_x, C_y	Torsional spring and damping constants which develop restoring moments to the "U" joint between the two rigid tower links.
K_B, C_B	The spring and damping constants of the torsional spring and dash pot connecting the transmission to the tower.

K_G, C_G	The spring and damping constants associated with the guy wires.
K_T, C_T	The torsional spring and damping constants which represent the lead-lag stiffness and damping of each blade (two springs/blade).

Again, note that these equations do not include gravitational effects. Also, in simplifying the first nine equations, the following approximations have been made:

$$\frac{u}{\ell}, \frac{v}{\ell} \leq .01 \; ; \; \frac{\dot{u}}{\ell}, \frac{\dot{v}}{\ell} = O(.1\,\Omega_z) \; ; \text{ and}$$

$$\frac{\ddot{u}}{\ell}, \frac{\ddot{v}}{\ell} = O(\Omega_z^2) \quad .$$

These are consistent with the approximations that have previously been made.

As stated above, the equations in Table 1 refer to a rotor which is connected to a synchronous generator. In this case, the angle, ϕ_o, is assumed to be proportional to time (constant angular velocity) corresponding to the synchronous speed of the generator. This assumption implies that the synchronous generator has small inertia and large electrical stiffness relative to the turbine polar inertia and torsional stiffness, respectively.

The rotor may also be connected to an induction generator, in which case the angle, ϕ_o, is unknown, but is governed by the equation

$$R^2 I_m \ddot{\varphi}_o = K_B(\varphi - \varphi_o) + C_B(\dot{\varphi} - \dot{\varphi}_o) + RT\{R\dot{\varphi}_o\} \quad . \tag{11}$$

In this equation, I_m is the moment of inertia of the high-speed drive-train components (including the generator armature), R is the speed-increase ratio of the transmission, and $T\left\{R\phi_o\right\}$ is the motor torque-speed function. For the generator used on the DOE/Sandia 17 m rotor, the torque-speed function is displayed graphically in Fig. 7. To implement the

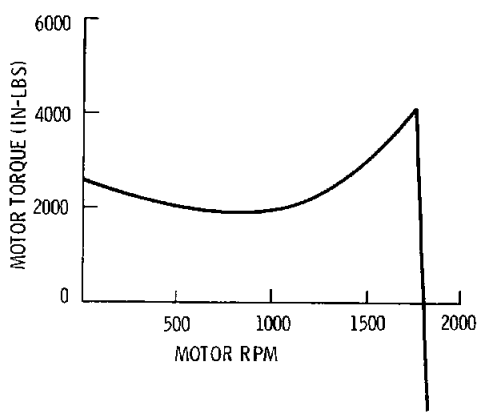

Figure 7: Torque-Speed Curve for the Generator Used on the DOE/Sandia 17 Meter Turbine

induction generator in the VAWTDYN model, Eq. (11) must be added to the set of equations given in Table 1.

The resultant moments, $M_{w_x}(\phi)$, $M_{w_x}(\phi+\pi)$, etc, developed by the aerodynamic wind loading on the blades are computed by integrating the moment per unit length about the lower attachment point, over the blade length. The load distribution from which the moments are derived is determined for a specified mean wind velocity and rotor RPM using a single streamtube aerodynamic model[7,8]. This model is strictly applicable only to steady conditions, where both the RPM and the wind velocity are constant. It should be noted that virtually any aerodynamic model which supplies the load resultants as functions of the angular position of the rotor may be readily incorporated into VAWTDYN.

The VAWTDYN package utilizes a "canned" integrator called "ODE," which was designed for the integration of coupled sets of nonlinear ordinary differential equations (initial value problems only). This routine employs a variable step-size scheme wherein the time step is altered from step to step to keep the local error per step within some prescribed tolerance. It is based on a variable-order Adams method, which adapts the order of integration to the problem dynamically.[9] Basically, ODE requires the user to provide both the initial conditions and the second derivatives of each degree of freedom as functions of the zeroth and first derivatives available at the completion of the previous time step. The latter requirement is accomplished by inserting the values of the

lower-order derivatives into the equations of Table 1 and numerically solving for the appropriate second-order derivatives.

VAWTDYN is equipped with the capability to "lock out" one or more degrees of freedom, i.e., to replace movable joints with rigid ones. This capability is important in effecting diagnostic tests and establishing which rotor motions in the response are dominant. A "lock out" is accomplished by first zeroing the appropriate degree of freedom along with all of its derivatives in the equations of Table 1. Then, terms which involve the degree of freedom multiplied by a spring constant are interpreted as the unknown force or moment necessary to restrain the motion and are transferred to the left-hand side of the equations. With these alterations to the equations, the "lock out" will be achieved. This method of "locking out" certain motions in the turbine is superior to the method of making specific spring constants arbitrarily large, since, as spring constants increase, so do frequencies, attended by numerical integration problems associated with automatic time-step selection based on the smallest period present in the motion.

For output processing, a general purpose plotting package has been incorporated in VAWTDYN. Variable versus variable plots, including time history plots, can be quickly and easily

generated. In addition, an option is available by which the frequency content of any of the time series can be obtained. Since this option involves the use of the Fast Fourier Transform, care must be taken to make the sampling rate sufficiently high to avoid aliasing of significant response frequencies which are above the Nyquist frequency.

The various input and output capabilities of VAWTDYN will be covered in greater detail in a future report devoted to software descriptions. This document will contain a listing of the program as well as instructions on its use.

Verification and Qualification of VAWTDYN

In order to develop confidence in any complex structural software package, two checkout activities are imperative. The first, termed verification, involves confirming that the software does what it is designed to do. One excellent way of accomplishing this is by comparing the software predictions with closed-form solutions, if available. The other checkout activity, called qualification, demonstrates that the software predicts with adequate accuracy the behavior of actual hardware. Good experimental data is crucial to this endeavor. Thus, the verification activity attempts to demonstrate coherence between the mathematical model and the software, whereas qualification demonstrates the coherence between the

mathematical model represented by the software and the actual hardware.

Two types of problems were used to verify VAWTDYN. The first involves investigating a form of the rotating turbine, wherein the turbine is transformed into a symmetrical spinning top by (1) decoupling it from the transmission, (2) converting the action of the tiedown cables to the action of gravity, and (3) setting $I_{xx} = I_{yy}$ and $I_{yz} = 0$. In addition, to produce a rigid turbine, the motions u, v, η, and ρ are "locked out". Due to the availability of closed-form solutions, spinning-top problems serve to verify the gyroscopic behavior as represented by the software.

In the first problem, the top is given a set of initial conditions such that the ensuing motion consists of precession without nutation. The equation which relates $\dot{\psi}$ to $\dot{\phi}$ and θ for this motion is given by

$$\dot{\psi} = \frac{\dot{\varphi}\,\bar{I}_{zz}}{2\cos\theta(\bar{I}_{zz} - \bar{I}_{xx})}\left\{-1 \pm \left[1 + \frac{4W\ell\cos\theta(\bar{I}_{zz} - \bar{I}_{xx})}{(\dot{\varphi}\,\bar{I}_{zz})^2}\right]^{\frac{1}{2}}\right\}, \qquad (12)$$

where the overbar on the moment-of-inertia terms denotes total values for the top, and W is the total weight of the top. For $\bar{I}_{xx} = 5.357 \times 10^5$ slug-ft^2, $\bar{I}_{zz} = 3.921 \times 10^4$ slug-ft^2, $W = 1.50 \times 10^4$ slugs, $\dot{\phi} = 10\pi$ rad/sec and

$\theta = 30°$, Eq. 12 yields $\dot{\Psi} = .394$ rad/sec. With these initial conditions, VAWTDYN predicts only minor variations from the initial values, as expected. In fact, after the precession angle, ψ, had reached 564°, the variability in the nutation angle, θ, is bracketed by 29.99988° and 30.00293°.

The next spinning-top verification problem involves combined precession and nutation. First, the top is set spinning with the initial angles of nutation and precession fixed, and subsequently released. For nonzero initial nutational angles, it can be shown from energy considerations that the top will precess and nutate in a scalloped pattern always returning at the end of each scallop to the initial nutational angle. With initial conditions of $\theta = 10°$ and $\dot{\phi} = 300$ rpm, the scalloped pattern predicted by VAWTDYN is shown in Fig. 8 where θ is plotted versus ψ. Note that the nutational angle varies between 10 and approximately 15 degrees, returning to 10° at the end of each scallop, as anticipated. The corresponding variation in ϕ is shown in Fig. 9. For the same initial conditions, but reducing I_{zz} by almost a factor of two, the nutational angle ranges from 10 to nearly 80 degrees (i.e., the top almost lays down), as shown in Fig. 10, with the corresponding variation in $\dot{\phi}$, shown in Figure 11.

The two problems above verify that the gyroscopic effects have been correctly incorporated in VAWTDYN.

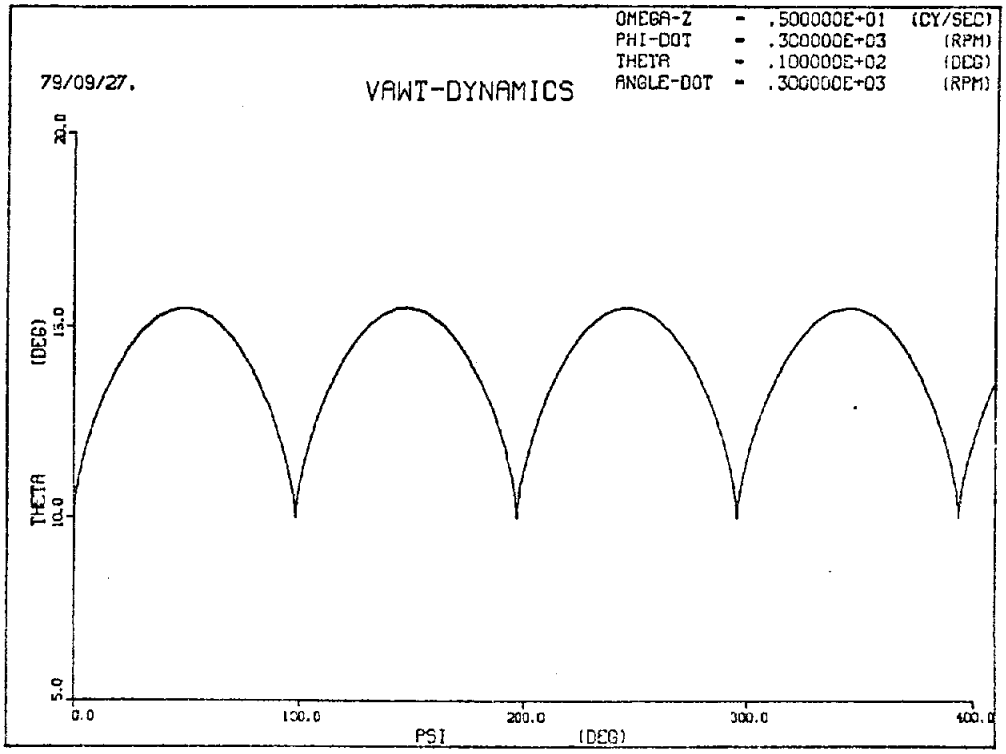

Figure 8: VAWTDYN Predictions of Nutational Angle, θ, Versus Precessional Angle, ψ, for a Symmetrical Top Spinning Initially at 300 rpm Released From an Initial Nutational Angle of 10° ($\bar{I}_{zz}$ = 3.921 x 10^4 slug-ft^2)

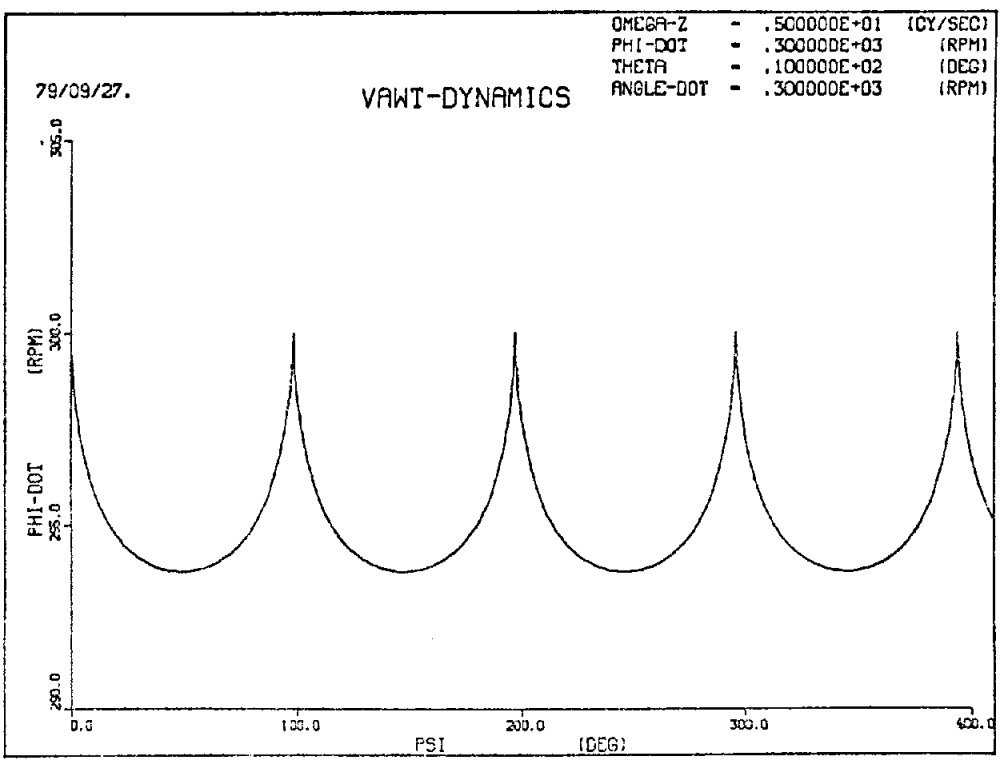

Figure 9: VAWTDYN Predictions of Spin Velocity, ϕ, Versus Precessional Angle, ψ, for a Symmetrical Top Spinning Initially at 300 rpm Released From an Initial Nutational Angle of 10° ($\bar{I}_{zz}$ = 3.921 x 10^4 slug-ft^2)

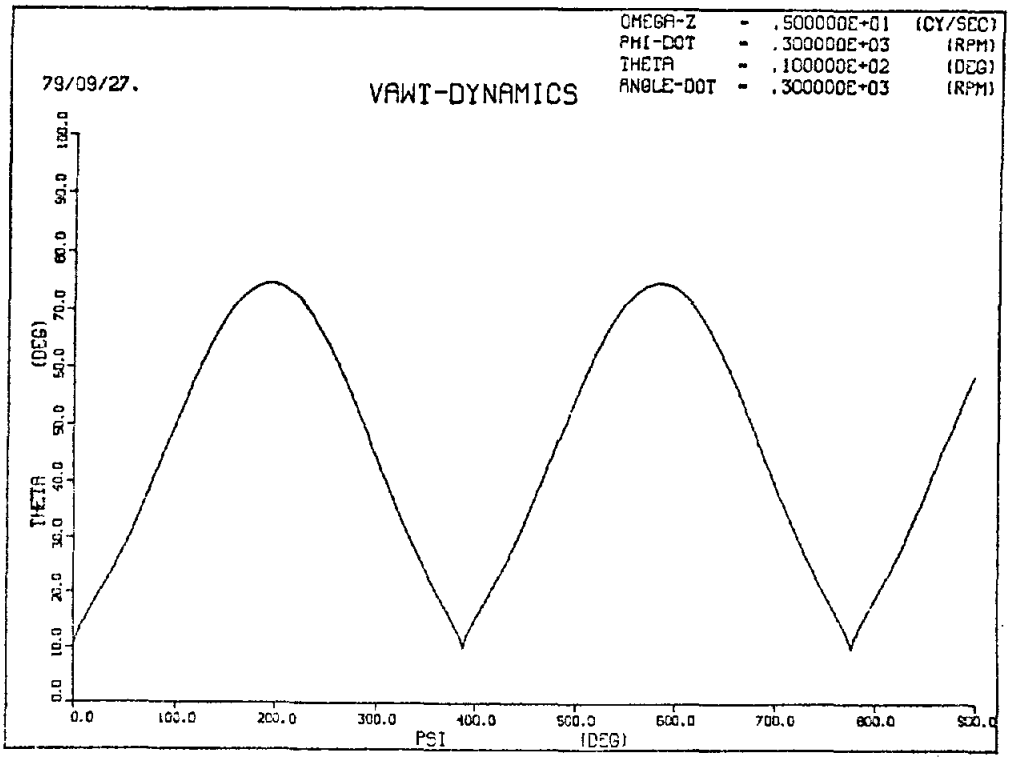

Figure 10: VAWTDYN Predictions of Nutational Angle, θ, Versus Precessional Angle, ψ, for a Symmetrical Top Spinning Initially at 300 rpm Released From an Initial Nutational Angle of 10° ($\bar{I}_{zz}$ = 2.425 x 10^4 slug-ft^2)

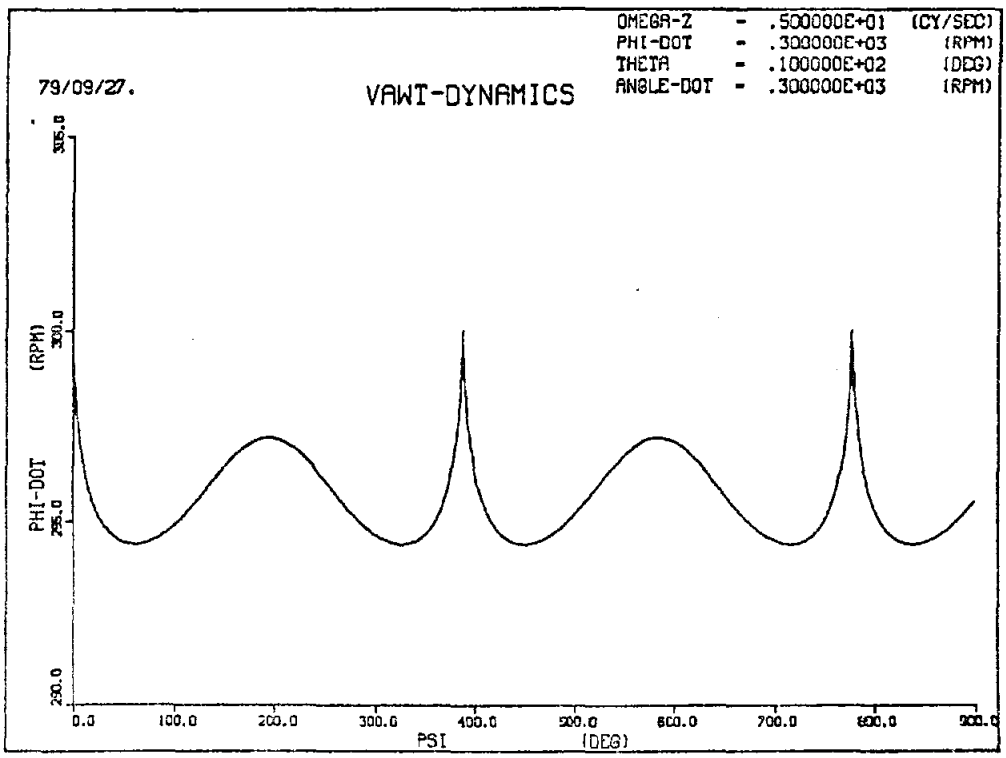

Figure 11: VAWTDYN Predictions of Spin Velocity, ϕ, Versus Precessional Angle, ψ, for a Symmetrical Top Spinning Initially at 300 rpm Released From an Initial Nutational Angle of 10° ($\bar{I}_{zz}$ = 2.425 x 10^4 slug-ft^2

To verify vibrational motion for the case of the parked turbine, VAWTDYN is exercised by displacing and then releasing the top of the non-rotating turbine such that all modes except the torsional ones are excited. This includes three modes with motion transverse to the blades (butterfly), and two with motion in the plane of the blades (in-plane). The spectrum of the predicted time series for U, the transverse motion of the midpoint of the tower, is shown in Fig. 12. The frequencies

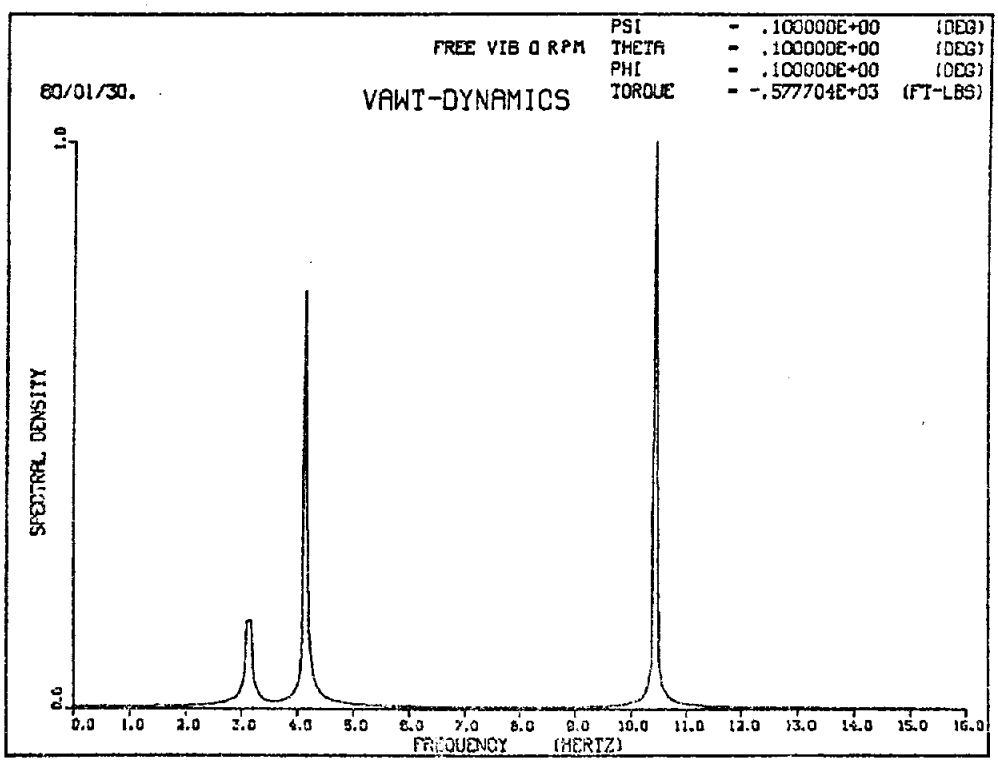

Figure 12: Spectrum of the Free Undamped Transverse Motion, U, for the Midpoint of the Tower as Predicted by VAWTDYN for the Parked Configuration

associated with the three well-defined spikes agree closely with those obtained from hand calculations using an analogous simplified spring-mass model of the transverse motion. The spectrum for V, the in-plane motion of the tower midpoint, shown in Fig. 13, contains two well-defined spikes as expected,

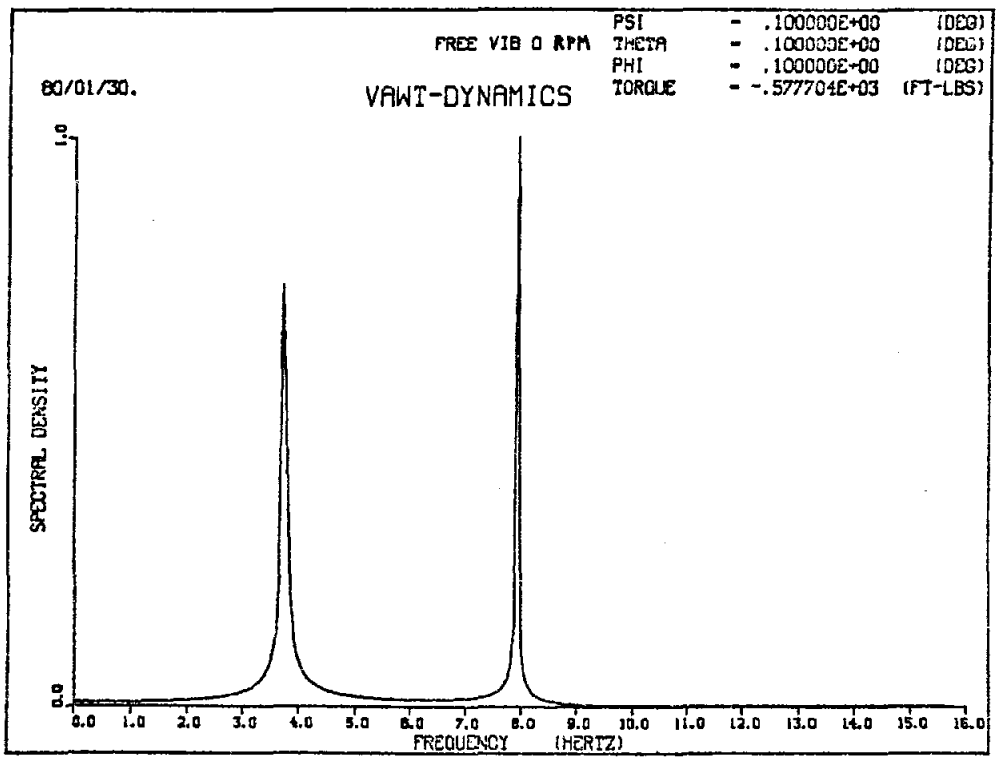

Figure 13: Spectrum of the Free Undamped In-Plane Motion, V, for the Midpoint of the Tower as Predicted by VAWTDYN for the Parked Configuration

which are also consistent with frequencies obtained from a simple spring-mass model. Similar correlation has been

obtained for the frequencies associated with the rotational degrees of freedom, ϕ and η, which are excited by releasing the parked rotor from a torsionally displaced position.

In addition to the above verification exercises, two preliminary qualification exercises have been performed using experimental data generated from the DOE/Sandia 17 meter turbine. Of course stiffness, damping, and mass properties in the model are chosen to correspond with available estimates of those in the experimental configuration. Although mass properties are easily calculable, stiffness properties are not. Therefore, in this case, the spring constants are adjusted so that the natural frequencies of the modes in the model match frequencies of corresponding modes determined by other methods. These other methods can range from simple "back-of-the-envelope" calculations to elaborate finite element computations. Frequencies obtained experimentally can also be used. Here, frequencies are determined through finite element calculations. Having established the spring constants in this manner, the damping is adjusted using the log-decrement technique until damping corresponding to 5% of critical is obtained.

In the first qualification exercise, low-speed-shaft torque data gathered while starting the 17 m rotor in low wind by applying full voltage to the induction motor/generator is compared to predictions by VAWTDYN. This test problem involves only the torsional modes of the model, which include the following degrees of freedom: the rotor spin angle, ϕ; blade propeller motion, $\eta = \alpha+\beta$; and the low-speed-shaft angle, ϕ_0. The model predictions and actual start-up data are shown in Figs. 14 and 15, respectively. The agreement is very

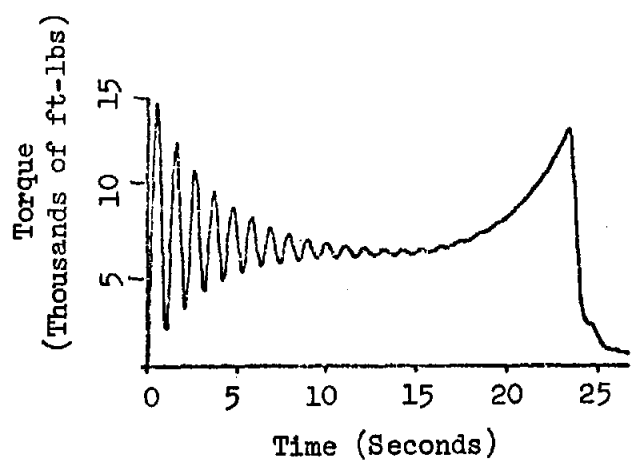

Figure 14: VAWTDYN Predictions of Low-Speed Shaft Torque Versus Time for Turbine Start-Up

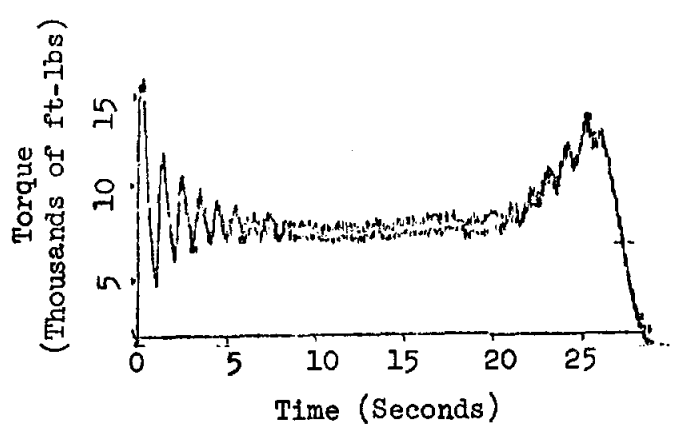

Figure 15: Experimental Low-Speed Shaft Torque Data for Start-Up

encouraging, though there are some notable differences. The start-up time is somewhat longer on the actual system, probably because of aerodynamic and/or frictional losses not included in the VAWTDYN model. The frequency of the oscillation following initial engagement of the motor is slightly lower than predicted. This is most likely due to inaccuracy in the selection of the spring constant, K_B. Even considering these differences, it is apparent that the model accurately identifies the major system-response features during rotor start-up.

In the second qualification exercise, vibratory stress amplitudes measured at the trailing edge of the blade near the root are compared to predictions by VAWTDYN. Since VAWTDYN does not normally compute stresses, the stresses are determined from the lead-lag moment at the root of the blade (which is equal to $K_T \alpha$) and a knowledge of the blade section properties. Although data was collected at a variety of wind speeds, the rotation of the rotor was fixed at 50.6 rpm for all cases. As shown in Fig. 16, the data contains a large amount of scatter. However, the VAWTDYN predictions, depicted by the solid curve, are in reasonable agreement with the data and, in general, are in much better agreement than the static predictions. Fine-tuning the model for a more accurate representation of the physical configuration may lead to better agreement.

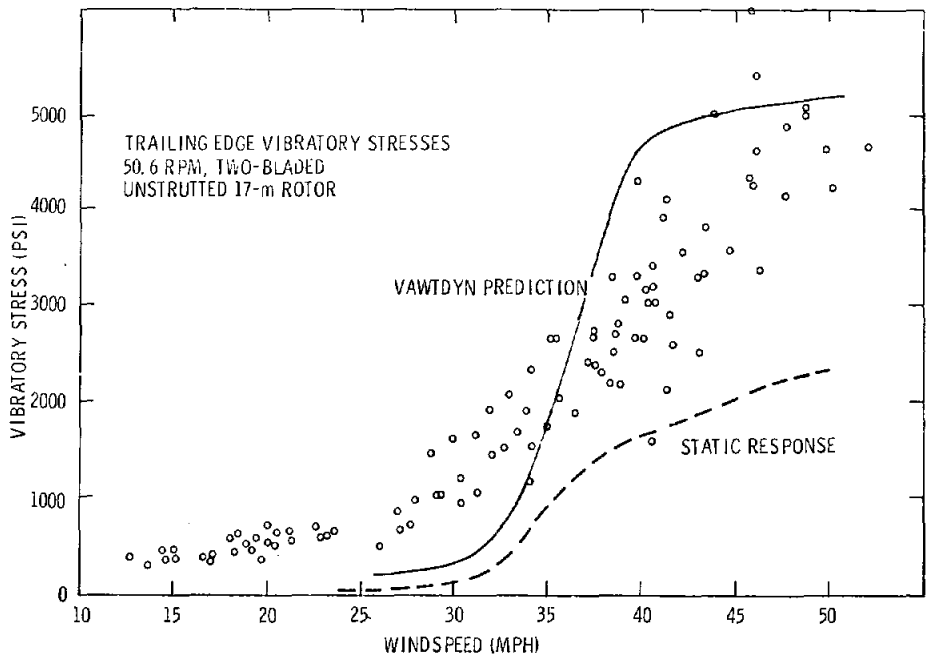

Figure 16: Comparison of VAWTDYN Predictions with Data for the Vibratory Stress Amplitudes at the Trailing Edge of the Blade Near the Root

This comparison is more significant than the start-up comparison discussed above because this test case involves virtually all the degrees of freedom in VAWTDYN, as well as the aerodynamic load model. While the agreement on stress amplitudes is very encouraging, more detailed comparisons are necessary to qualify the model. Specifically, comparisons should be made at other rotor RPM's and spectral details of the predicted and measured strain time series should be examined. These activities are being pursued and will be discussed in follow-up reports.

The qualification exercises outlined above, coupled with the prior verification problems, serve to generate some confidence

that VAWTDYN solves correctly those problems for which it was developed, and furthermore, that the model is capable of predicting with reasonable accuracy, the dynamic behavior of real VAWT systems. The qualification activities will be ongoing, expecially as additional experimental data becomes available.

Capabilities of the Model

Having developed some confidence in the model, it is appropriate to discuss some of its capabilities and consequences.

The model can be used to determine resonant frequencies for the primary system vibrational modes as a function of rotational speed. This is accomplished by exciting the model through initial conditions and obtaining spectral analysis of the resulting displacement variable time series.

For the non-rotating case, the seven mode shapes along with their appropriate frequencies and identification labels, are indicated graphically in Fig. 17. These modes are quite representative of the lowest modes of vibration in the DOE/Sandia 17-m two-bladed Darrieus rotor, with the exception of in-plane blade modes which are not represented in the model. The spring and mass values in VAWTDYN are selected to provide similar frequencies and mode shapes as predicted by finite element analysis of the 17-m rotor.

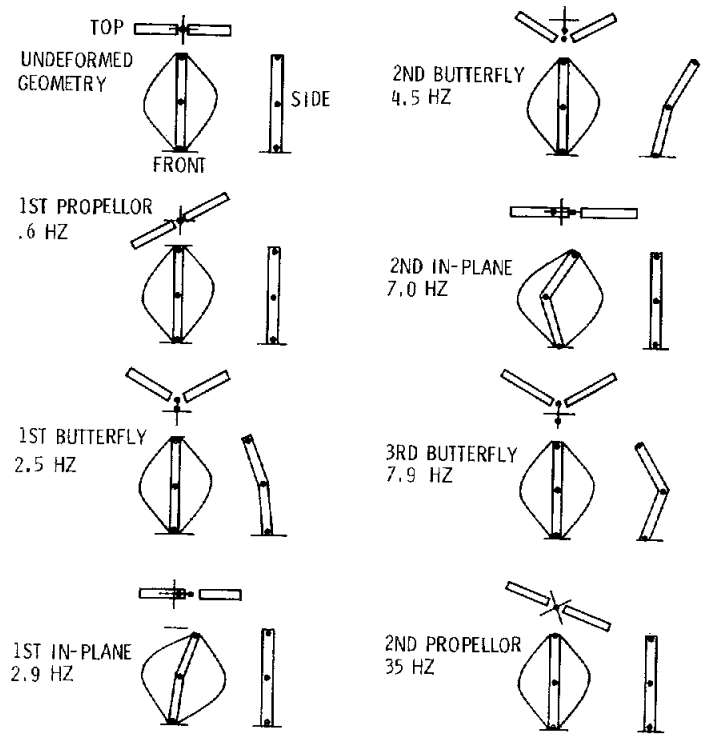

Figure 17: Mode Shapes and Associated Frequencies of the VAWTDYN Model in a Non-Rotating Condition

The effect of rotor rotation on the frequencies of vibration is shown in Fig. 18. This plot is determined from free, undamped vibration spectra of the u, v, α, and β degree of freedom. Thus, these frequencies represent those which would be measured by an observer fixed to the xyz coordinates, i.e., an observer fixed to the rotating tower. There are substantial upward or downward changes in frequency of certain rotor modes. These frequency changes are roughly proportional to rotor rpm and are the order of 1 per rev in magnitude. This result is caused by the coriolis and centrifugal terms in VAWTDYN and is similar to classical shaft whirl effects.

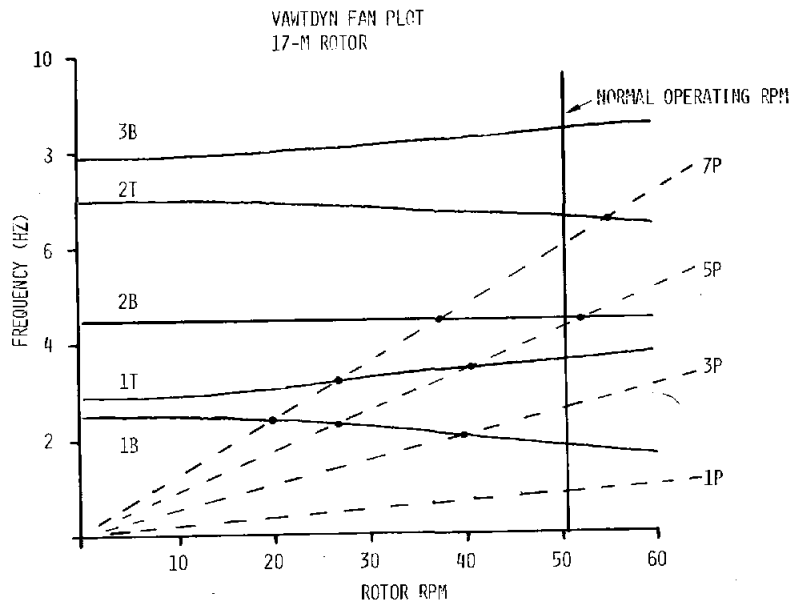

Figure 18: Fan Plot for the VAWTDYN Model

Apparently, the modes dominated by tower motion (e.g., the first butterfly and first in-plane mode) are most affected by this phenomenon.

Also shown in Fig. 18 are fan lines corresponding to odd per revolution harmonics of the aerodynamic forcing functions. Even per rev harmonics are not shown because the aerodynamic force components capable of exciting the modes in Fig. 18 have only odd harmonics relative to the xyz system. This may be deduced from the fact that load resultants measured relative to the fixed XYZ system have only even harmonics due to the symmetry of the two-bladed rotor.

Critical rotor speeds corresponding to crossings of the fan lines with rotor natural frequencies will produce resonances, the significance of which depends on the harmonic magnitudes of the forcing functions. It is noteworthy that identification of critical rotor speeds can be in substantial error if the frequency shifts due to coriolis or centrifugal effects are neglected.

Rotor rotation also affects the system mode shapes. Figures 12 and 13 display the u (out-of-plane) and v (in-plane) spectra for free vibrations of a parked rotor. The spectral spikes for each mode of vibration involve either u or v motions, but not both, indicating independence of the in-plane and out-of-plane motions. Figures 19 and 20 are a similar comparison of spectra for a turbine rotating at normal operating speed. In this case, spectral spikes in the u variable also appear in the v variable, indicating that each vibrational mode on the turning rotor generally involves both in-plane and out-of-plane motions. Recognition of this coupling is important in establishing when a system will resonate. For example, a purely in-plane mode on a stationary rotor can be excited by out-of-plane forces when the system is operating due to coupling of the u and v motions.

VAWTDYN can be used to determine steady state forced vibration response such as that shown in Fig. 17. These solutions

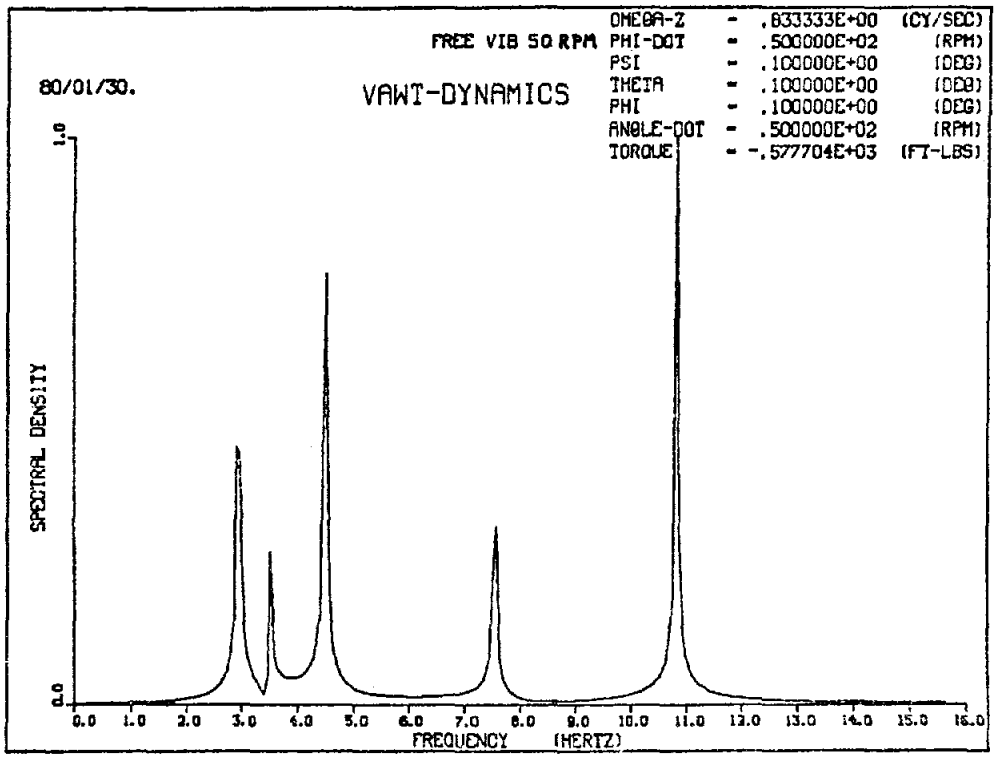

Figure 19: Spectrum of the Free Undamped Transverse Motion, U, for the Midpoint of the Tower as Predicted by VAWTDYN for the Turbine Rotating at 50 rpm

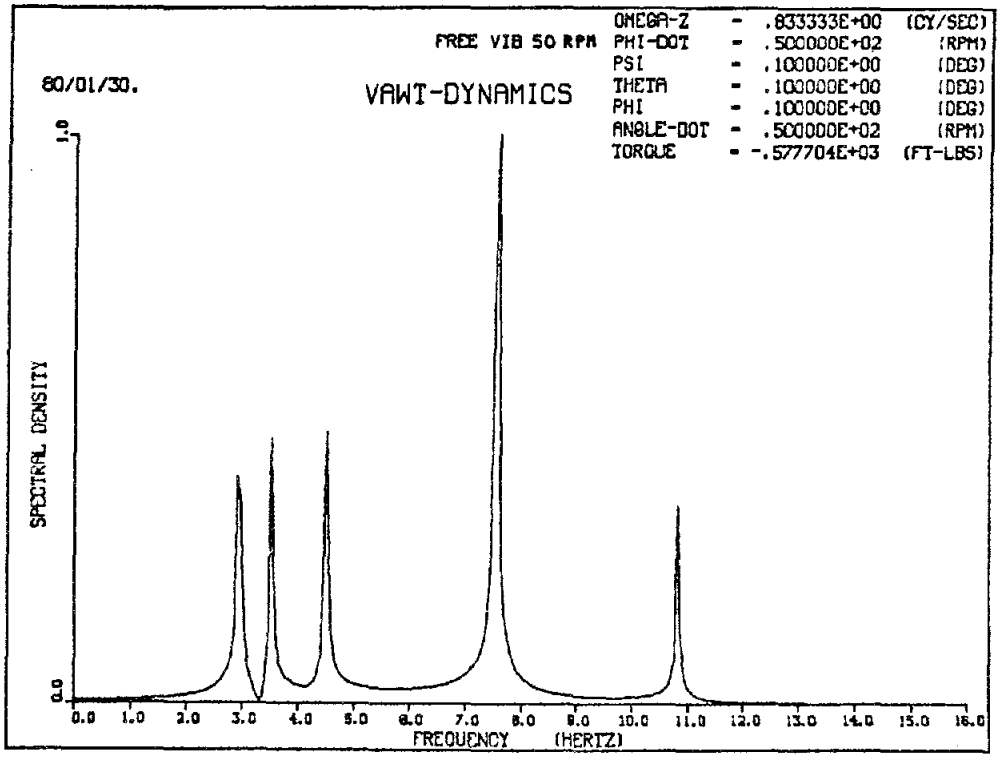

Figure 20: Spectrum of the Free Undamped In-Plane Motion, V, for the Midpoint of the Tower as Predicted by VAWTDYN for the Turbine Rotating at 50 rpm

are obtained by suddenly applying the aerodynamic loads with the system initially rotating at synchronous speed. The system reaches steady state after the transients decay (generally within several rotor revolutions for 5% of critical structural damping). From the steady state solution, all the VAWTDYN variable amplitudes and spectral characteristics may be determined. The effects of rotor speed, windspeed, and rotor component stiffness or mass on any aspect of system response modeled by VAWTDYN may be readily estimated. Torque ripple[10] effects may also be determined within the accuracy of the drive train model included in VAWTDYN.

As VAWTDYN is basically a transient model, transient response, such as the startup problem discussed previously, is within the capability of the model. Response of the system to time varying gusts at operating speed is possible to analyze with the qualification that the aerodynamic load model is based on steady-state aerodynamics. On very large systems where the gust rise time is short relative to the rotor revolution period, unsteady aerodynamic effects may be important and appropriate modifications to the load model should be considered.

Summary and Conclusions

In the preceding sections, the model from which VAWTDYN was developed has been described, some efforts have been made to

verify the software and qualify the model, and finally, discussion of the model's capabilities has been presented. The qualification and verification activities have served to generate confidence that VAWTDYN can reasonably predict the dynamic behavior of VAWT's both qualitatively and quantitatively, and, along with the discussion of capabilities, the utility of the VAWTDYN package has been demonstrated.

The model indicates that significant dynamic amplification of rotor response can occur under certain conditions. The ability of the model to predict these amplifications can substantially impact future system designs by identifying areas of structural over- or under-design. For over-design situations, alternatives proposed to eliminate the excess (thereby reducing costs) can be evaluated with VAWTDYN and, of course, in the case of under-design, successful corrective measures can be identified.

It should be emphasized that VAWTDYN in its current form contains many approximations which may preclude its use for certain aspects of dynamic design. Potential users should be familiar enough with the underlying theory in the model to avoid misusing it. Efforts will continue in the future to establish the strengths and limitations of VAWTDYN by making more detailed comparisons with the 17 m rotor data.

Future development activities include extending the model to a three-bladed rotor such that analyses can be carried out on some three-bladed designs which are under current consideration; incorporating flatwise-blade motions in the model for the accurate analysis of turbines in which this motion may be more predominant, e.g., turbines with larger height-to-diameter ratios than the 17 m turbine; and making necessary alterations for analyzing cantilevered VAWT designs.

Whether or not any or all of these activities will be pursued will depend upon the continued success of the current package and on the presence of a demand for the specific development activity.

References

1. W. N. Sullivan, "Structural Loads for the 17-m Darrieus Turbine," Vertical Axis Wind Turbine Technology Workshop, May 17-20, 1976, Sandia Laboratories, SAND76-5586.

2. L. I. Weingarten, D. W. Lobitz, "Blade Structural Analysis," Vertical Axis Wind Turbine Technology Workshop, May 17-20, 1976, Sandia Laboratories, SAND76-5586.

3. W. N. Sullivan, "Operational Experience with VAWT Blades at Sandia Laboratories," Proc. of the DOE/NASA Workshop on Large Wind Turbine Design Characteristics and R & D Requirements (to be published), Cleveland, April 24-26, 1979.

4. K. R. V. Kaza, D. C. Janetzke, and T. L. Sullivan, "Evaluation of MOSTAS Computer Code for Predicting Dynamic Loads in Two-Bladed Wind Turbines," National Aeronautics and Space Administration, DOE/NASA/1028-79/2, NASA TM-79101, April 1979.

5. H. H. Ottens and R. J. Zwaan, "Description of a Method to Calculate the Aeroelastic Stability of a Vertical Axis Wind Turbine," National Aerospace Laboratory NLR, The Netherlands, NLR TR 78072 L, June 1978.

6. A. J. Vollan and R. J. Zwaan, "Contribution of NLR to the First Phase of the National Research Program on Wind Energy, Part II: Elastomechanical and Aeroelastic Stability," National Aerospace Laboratory NLR, The Netherlands, NLR TR 77030 U Part II, March 1977.

7. R. J. Templin, "Aerodynamic Performance Theory for the NRC Vertical Axis Wind Turbine," National Research Council, Canada, LTR-LA-160, June 1974.

8. J. H. Strickland, "The Darrieus Turbine: A Performance Prediction Model Using Multiple Streamtubes," Sandia Laboratories, SAND75-0431, October 1975.

9. L. F. Shampine and M. K. Gordon, Computer Solution of Ordinary Differential Equations: The Initial Value Problem, W. H. Freeman and Co., San Francisco, 1975.

10. R. C. Reuter, Jr. and M. H. Worstell, "Torque Ripple in a Vertical Axis Wind Turbine," Sandia Laboratories, SAND78-0577, April, 1978.

Due to algebraic complexity, the expansion of Eq. (5) in the model description section of this report is presented in this appendix. The terms of this equation are expanded individually below:

$$\left(\frac{d\underset{\sim}{H}_A}{dt}\right)_{xyz} = \left(\frac{d\underset{\approx}{I}(\alpha)}{dt}\right)_{xyz} \underset{\sim}{\omega} + \underset{\approx}{I}(\alpha)\left(\frac{d\underset{\sim}{\omega}}{dt}\right)_{xyz}$$

$$= \begin{Bmatrix} (I_{yy} - I_{xx})\, 2\sin\alpha\cos\alpha\dot{\alpha}\,\Omega_x + (I_{yy} - I_{xx})(\cos^2\alpha - \sin^2\alpha)\,\dot{\alpha}\Omega_y - I_{yz}\cos\alpha\dot{\alpha}(\Omega_z + \dot{\alpha}) \\ (I_{yy} - I_{xx})(\cos^2\alpha - \sin^2\alpha)\,\dot{\alpha}\Omega_x + (I_{xx} - I_{yy})\, 2\sin\alpha\cos\alpha\dot{\alpha}\Omega_y + I_{yz}\sin\alpha\dot{\alpha}(\Omega_z + \dot{\alpha}) \\ - I_{yz}\cos\alpha\dot{\alpha}\Omega_x + I_{yz}\sin\alpha\dot{\alpha}\Omega_y \end{Bmatrix}$$

$$+ \begin{Bmatrix} (I_{xx}\cos^2\alpha + I_{yy}\sin^2\alpha)\,\dot{\Omega}_x + (I_{yy} - I_{xx})\sin\alpha\cos\alpha\dot{\Omega}_y - I_{yz}\sin\alpha(\dot{\Omega}_z + \ddot{\alpha}) \\ (I_{yy} - I_{xx})\sin\alpha\cos\alpha\dot{\Omega}_x + (I_{xx}\sin^2\alpha + I_{yy}\cos^2\alpha)\dot{\Omega}_y - I_{yz}\cos\alpha(\dot{\Omega}_z + \ddot{\alpha}) \\ - I_{yz}\sin\alpha\dot{\Omega}_x - I_{yz}\cos\alpha\dot{\Omega}_y + I_{zz}(\dot{\Omega}_z + \ddot{\alpha}) \end{Bmatrix},$$

and,

$$\underset{\sim}{\Omega} \times \underset{\sim}{H}_A$$

$$= \begin{Bmatrix} \Omega_y[-I_{yz}\sin\alpha\Omega_x - I_{yz}\cos\alpha\Omega_y + I_{zz}(\Omega_z + \dot{\alpha})] \\ \quad -(\Omega_z + \dot{\alpha})[(I_{yy} - I_{xx})\sin\alpha\cos\alpha\Omega_x + (I_{xx}\sin^2\alpha + I_{yy}\cos^2\alpha)\,\Omega_y - I_{yz}\cos\alpha(\Omega_z + \dot{\alpha})] \\ (\Omega_z + \dot{\alpha})[(I_{xx}\cos^2\alpha + I_{yy}\sin^2\alpha)\Omega_x + (I_{yy} - I_{xx})\sin\alpha\cos\alpha\Omega_y - I_{yz}\sin\alpha(\Omega_z + \dot{\alpha})] \\ \quad - \Omega_x[-I_{yz}\sin\alpha\Omega_x - I_{yz}\cos\alpha\Omega_y + I_{zz}(\Omega_z + \dot{\alpha})] \\ \Omega_x[(I_{yy} - I_{xx})\sin\alpha\cos\alpha\Omega_x + (I_{xx}\sin^2\alpha + I_{yy}\cos^2\alpha)\,\Omega_y - I_{yz}\cos\alpha(\Omega_z + \dot{\alpha})] \\ \quad - \Omega_y[(I_{xx}\cos^2\alpha + I_{yy}\sin^2\alpha)\,\Omega_x + (I_{yy} - I_{xx})\sin\alpha\cos\alpha\Omega_y - I_{yz}\sin\alpha(\Omega_z + \dot{\alpha})] \end{Bmatrix}.$$

Eq. (6) in the model definition section is obtained from the above equations by eliminating the higher-order terms and making certain other approximations as outlined in that section of the report.

DISTRIBUTION:

TID-4500-R66 UC-60 (283)

Aero Engineering Department (2)
Wichita State University
Wichita, KS 67208
Attn: M. Snyder
W. Wentz

R. E. Akins, Assistant Professor
Department of Engineering Science
and Mechanics
Virginia Polytechnic Institute and
State University
Blacksburg, VA 24060

Alcoa Laboratories (5)
Alcoa Technical Center
Aluminum Company of America
Alcoa Center, PA 15069
Attn: D. K. Ai
A. G. Craig
J. T. Huang
J. R. Jombock
P. N. Vosburgh

Mr. Robert B. Allen
General Manager
Dynergy Corporation
P.O. Box 428
1269 Union Avenue
Laconia, NH 03246

American Wind Energy Association
54468 CR31
Bristol, IN 46507

E. E. Anderson
South Dakota School of Mines
and Technology
Department of Mechanical Engineering
Rapid City, SD 57701

Scott Anderson
318 Millis Hall
University of Vermont
Burlington, VT 05405

G. T. Ankrum
DOE/Office of Commercialization
20 Massachusetts Avenue NW
Mail Station 2221C
Washington, DC 20585

Holt Ashley
Stanford University
Department of Aeronautics and
  Astronautics Mechanical Engineering
Stanford, CA 94305

Kevin Austin
Consolidated Edison Company of
  New York, Inc.
4 Irving Place
New York, NY 10003

F. K. Bechtel
Washington State University
Department of Electrical Engineering
College of Engineering
Pullman, WA 99163

M. E. Beecher
Arizona State University
Solar Energy Collection
University Library
Tempe, AZ 85281

K. Bergey
University of Oklahoma
Aero Engineering Department
Norman, OK 73069

Steve Blake
Wind Energy Systems
Route 1, Box 93-A
Oskaloosa, KS 66066

Robert Brulle
McDonnell-Douglas
P.O. Box 516
Department 341, Building 32/2
St. Louis, MO 63166

R. Camerero
Faculty of Applied Science
University of Sherbrooke
Sherbrooke, Quebec
CANADA J1K 2R1

CERCEM
49 Rue du Commandant Rolland
93350 Le Bourget
FRANCE
Attn: G. Darrieus
       J. Delassus

Professor V. A. L. Chasteau
School of Engineering
University of Auckland
Private Bag
Auckland, NEW ZEALAND

Howard T. Clark
McDonnell Aircraft Corporation
P.O. Box 516
Department 337, Building 32
St. Louis, MO 63166

Dr. R. N. Clark
USDA, Agricultural Research Service
Southwest Great Plains Research Center
Bushland, TX 79012

Joan D. Cohen
Consumer Outreach Coordinator
State of New York
Executive Department
State Consumer Protection Board
99 Washington Avenue
Albany, NY 12210

Dr. D. E. Cromack
Associate Professor
Mechanical and Aerospace Engineering
Department
University of Massachusetts
Amherst, MA 01003

Gale B. Curtis
Tumac Industries
650 Ford Street
Colorado Springs, CO 80915

DOE/ALO (3)
Albuquerque, NM 87185
Attn: G. P. Tennyson
D. C. Graves
D. W. King

DOE Headquarters (20)
Washington, DC 20545
Attn: L. V. Divone, Chief
Wind Systems Branch
D. F. Ancona, Program Manager
Wind Systems Branch

C. W. Dodd
School of Engineering
Southern Illinois University
Carbondale, IL 62901

Dominion Aluminum Fabricating Ltd. (2)
3570 Hawkestone Road
Mississauga, Ontario
CANADA L5C 2U8
Attn: L. Schienbein
C. Wood

D. P. Dougan
Hamilton Standard
1730 NASA Boulevard
Room 207
Houston, TX 77058

J. B. Dragt
Nederlands Energy Research Foundation (E.C.N.)
Physics Department
Westerduinweg 3 Patten (nh)
THE NETHERLANDS

C. E. Elderkin
Battelle-Pacific Northwest Laboratory
P.O. Box 999
Richland, WA 99352

Frank R. Eldridge, Jr.
The Mitre Corporation
1820 Dolley Madison Blvd.
McLean, VA 22102

Electric Power Research Institute
3412 Hillview Avenue
Palo Alto, CA 94304
Attn: E. Demeo'

James D. Fock, Jr.
Department of Aerospace Engineering Sciences
University of Colorado
Boulder, CO 80309

Dr. Lawrence C. Frederick
Public Service Company of New Hampshire
1000 Elm Street
Manchester, NH 03105

E. Gilmore
Amarillo College
Amarillo, TX 79100

Paul Gipe
Wind Power Digest
P.O. Box 539
Harrisburg, PA 17108

Roger T. Griffiths
University College of Swansea
Department of Mechanical Engineering
Singleton Park
Swansea SA2 8PP
UNITED KINGDOM

Professor N. D. Ham
Massachusetts Institute of Technology
77 Massachusetts Avenue
Cambridge, MA 02139

Sam Hansen
DOE/DST
20 Massachusetts Avenue
Washington, DC 20545

C. F. Harris
Wind Engineering Corporation
Airport Industrial Area
Box 5936
Lubbock, TX 79415

W. L. Harris
Aero/Astro Department
Massachusetts Institute of Technology
Cambridge, MA 02139

Terry Healy (2)
Rocky Flats Plant
P.O. Box 464
Golden, CO 80401

Helion
P.O. Box 4301
Sylmar, CA 91342

Don Hinrichsen
Associate Editor
AMBIO
KVA
Fack, S-10405
Stockholm
SWEDEN

Sven Hugosson
Box 21048
S. 100 31 Stockholm 21
SWEDEN

O. Igra
Department of Mechanical Engineering
Ben-Gurion University of the Negev
Beer-Sheva, ISRAEL

Indian Oil Corporation, Ltd.
Marketing Division
254-C, Dr. Annie Besant Road
Prabhadevi, Bombay-400025
INDIA

JBF Scientific Corportion
2 Jewel Drive
Wilmington, MA 01887
Attn: E. E. Johanson

Dr. Gary L. Johnson, P.E.
Electrical Engineering Department
Kansas State University
Manhattan, KS 66506

J. P. Johnston
Stanford University
Department of Mechanical Engineering
Stanford, CA 94305

B. O. Kaddy, Jr.
Box 353
31 Union Street
Hillsboro, NH 03244

Kaman Aerospace Corporation
Old Windsor Road
Bloomfield, CT 06002
Attn: W. Batesol

Robert E. Kelland
The College of Trades and Technology
P.O. Box 1693
Prince Philip Drive
St. John's, NEWFOUNDLAND
A1C 5P7

Larry Kinnett
P.O. Box 6593
Santa Barbara, CA 93111

O. Krauss
Michigan State University
Division of Engineering Research
East Lansing, MI 48824

Lawrence Livermore Laboratory
P.O. Box 808 L-340
Livermore, CA 94550
Attn: D. W. Dorn

M. Lechner
Public Service Company of New Mexico
P.O. Box 2267
Albuquerque, NM 87103

G. G. Leigh
UNM/CERF
P.O. Box 188
University Station
Albuquerque, NM 87131

George E. Lennox
Industry Director
Mill Products Division
Reynolds Metals Company
6601 West Broad Street
Richmond, VA 23261

J. Lerner
State Energy Commission
Research and Development Division
1111 Howe Avenue
Sacramento, CA 95825

L. Liljidahl
Building 303
Agriculture Research Center
USDA
Beltsville, MD 20705

P. B. S. Lissaman
Aeroenvironment, Inc.
660 South Arroyo Parkway
Pasadena, CA 91105

Olle Ljungstrom
FFA, The Aeronautical Research Institute
Box 11021
S-16111 Bromma
SWEDEN

Los Alamos Scientific Laboratories
P.O. Box 1663
Los Alamos, NM 87544
Attn: J. D. Balcomb Q-DO-T
Library

Ernel L. Luther
Senior Associate
PRC Energy Analysis Co.
7600 Old Springhouse Rd.
McLean, VA 22101

L. H. J. Maile
48 York Mills Rd.
Willowdale, Ontario
CANADA M2P 1B4

Jacques R. Maroni
Ford Motor Company
Environmental Research and Energy
  Planning Director
Environmental and Safety Engineering Staff
The American Road
Dearborn, MI 48121

Frank Matanzo
Dardalen Associates
15110 Frederick Road
Woodbine, MD 21797

J. R. McConnell
Tumac Industries, Inc.
650 Ford St.
Colorado Springs, CO 80915

James Meiggs
Kaman Sciences Corporation
P.O. Box 7463
Colorado Springs, CO 80933

R. N. Meroney
Colorado State University
Department of Civil Engineering
Fort Collins, CO 80521

G. N. Monsson
Department of Economic Planning
  and Development
Barrett Building
Cheyenne, WY 82002

NASA Lewis Research Center (2)
21000 Brookpark Road
Cleveland, OH 44135
Attn: J. Savino, MS 509-201
R. L. Thomas
W. Robbins
K. Kaza, MS 49-6

V. Nelson
West Texas State University
Department of Physics
P.O. Box 248
Canyon, TX 79016

Leander Nichols
Natural Power, Inc.
New Boston, NH 03070

Oklahoma State University (2)
Stillwater, OK 76074
Attn: W. L. Hughes
EE Department
D. K. McLaughlin
ME Department

Oregon State University (2)
Corvallis, OR 97331
Attn: R. Wilson
ME Department
R. W. Thresher
ME Department

Pat F. O'Rourke
Precinct 4
County Commissioner
City-County Building
El Paso, TX 79901

H. H. Paalman
Dow Chemical USA
Research Center
2800 Mitchell Drive
Walnut Creek, CA 94598

R. A. Parmelee
Northwestern University
Department of Civil Engineering
Evanston, IL 60201

Helge Petersen
Riso National Laboratory
DK-4000 Roskilde
DENMARK

Wilson Prichett, III
National Rural Electric Cooperative
Association
1800 Massachusetts Avenue NW
Washington, DC 20036

Dr. Barry Rawlings, Chief
Division of Mechanical Engineering
Commonwealth Scientific and Industrial
Research Organization
Graham Road, Highett
Victoria, 3190
AUSTRALIA

Thomas W. Reddoch
Associate Professor
Department of Electrical Engineering
The University of Tennessee
Knoxville, TN 37916

A. Robb
Memorial University of Newfoundland
Faculty of Engineering and Applied Sciences
St. John's Newfoundland
CANADA A1C 5S7

Dr.-Ing. Hans Ruscheweyh
Institut fur Leichtbau
Technische Hochschule Aachen
Wullnerstrasse 7
GERMANY

Gwen Schreiner
Librarian
National Atomic Museum
Albuquerque, NM 87185

Arnan Seginer
Professor of Aerodynamics
Technion-Israel Institute of
Technology
Department of Aeronautical
Engineering
Haifa, ISRAEL

Dr. Horst Selzer
Dipl.-Phys.
Wehrtechnik und Energieforschung
ERNO-Raumfahrttechnik GmbH
Hunefeldstr. 1-5
Postfach 10 59 09
2800 Bremen 1
GERMANY

H. Sevier
Rocket and Space Division
Bristol Aerospace Ltd.
P.O. Box 874
Winnipeg, Manitoba
CANADA R3C 2S4

P. N. Shankar
Aerodynamics Division
National Aeronautical Laboratory
Bangalore 560017
INDIA

David Sharpe
Kingston Polytechnic
Canbury Park Road
Kingston, Surrey
UNITED KINGDOM

D. G. Shepherd
Cornell University
Sibley School of Mechanical and
Aerospace Engineering
Ithaca, NY 14853

Dr. Fred Smith
Mechanical Engineering Department Head
Colorado State University
Ft. Collins, CO 80521

Kent Smith
Instituto Technologico Costa Rica
Apartado 159 Cartago
COSTA RICA

Leo H. Soderholm
Iowa State University
Agricultural Engineering, Room 213
Ames, IA 50010

Southwest Research Institute (2)
P.O. Drawer 28501
San Antonio, TX 78284
Attn: W. L. Donaldson, Senior Vice President
R. K. Swanson

Rick Stevenson
Route 2
Box 85
Springfield, MO 65802

Dale T. Stjernholm, P.E.
Mechanical Design Engineer
Morey/Stjernholm and Associates
1050 Magnolia Street
Colorado Springs, CO 80907

G. W. Stricker
383 Van Gordon 30-559
Lakewood, CO 80228

C. J. Swet
Route 4
Box 358
Mt. Airy, MD 21771

R. J. Templin (3)
Low Speed Aerodynamics Section
NRC-National Aeronautical Establishment
Ottawa 7, Ontario
CANADA K1A OR6

Texas Tech University (3)
P.O. Box 4289
Lubbock, TX 79409
Attn: K. C. Mehta, CE Department
J. Strickland, ME Department
J. Lawrence, ME Department

Fred Thompson
Atari, Inc.
155 Moffett Park Drive
Sunnyvale, CA 94086

United Engineers and Constructors, Inc.
Advanced Engineering Department
30 South 17th Street
Philadelphia, PA 19101
Attn: A. J. Karalis

University of New Mexico (2)
Albuquerque, NM 87106
Attn: K. T. Feldman
Energy Research Center
V. Sloglund
ME Department

Jan Vacek
Eolienne experimentale
C.P. 279, Cap-aux-Meules
Iles de la Madeleine, Quebec
CANADA

Irwin E. Vas
Solar Energy Research Institute
1617 Cole Blvd.
Golden, CO 80401

Otto de Vries
National Aerospace Laboratory
Anthony Fokkerweg 2
Amsterdam 1017
THE NETHERLANDS

R. Walters
West Virginia University
Department of Aero Engineering
1062 Kountz Avenue
Morgantown, WV 26505

E. J. Warchol
Bonneville Power Administration
P.O. Box 3621
Portland, OR 97225

D. F. Warne, Manager
Energy and Power Systems
ERA Ltd.
Cleeve Rd.
Leatherhead
Surrey KT22 7SA
ENGLAND

R. A. Watson
Stanford University
546B Crothers Memorial Hall
Stanford, CA 94305

R. J. Watson
Watson Bowman Associates, Inc.
1280 Niagara St.
Buffalo, NY 14213

R. G. Watts
Tulane University
Department of Mechanical Engineering
New Orleans, LA 70018

Pat Weis
Solar Energy Research Institute
1536 Cole Blvd.
Golden, CO 80401

W. G. Wells, P.E.
Associate Professor
Mechanical Engineering Department
Mississippi State University
Mississippi State, MS 39762

T. Wentink, Jr.
University of Alaska
Geophysical Institute
Fairbanks, AK 99701

West Texas State University
Government Depository Library
Number 613
Canyon, TX 79015

Wind Energy Report
Box 14
104 S. Village Ave.
Rockville Centre, NY 11571
Attn: Farrell Smith Seiler

Richard E. Wong
Assistant Director
Central Solar Energy Research
  Corporation
1200 Sixth Street
328 Executive Plaza
Detroit, MI 48226

1000 G. A. Fowler
1200 L. D. Smith
3141 T. L. Werner (5)
3151 W. L. Garner (3)
For DOE/TIC (Unlimited Release)
3161 J. E. Mitchell (15)
3161 P. S. Wilson
4533 J. W. Reed
4700 J. H. Scott
4710 G. E. Brandvold
4715 R. H. Braasch (100)
4715 R. D. Grover
4715 E. G. Kadlec
4715 M. T. Mattison
4715 R. O. Nellums
4715 W. N. Sullivan
4715 M. H. Worstell
5500 O. E. Jones
5510 D. B. Hayes
5520 T. B. Lane
5521 D. W. Lobitz
5523 R. C. Reuter Jr.
5523 T. G. Carne
5530 W. Herrmann
5600 D. B. Schuster
5620 M. M. Newsom
5630 R. C. Maydew
5632 C. W. Peterson
5632 P. C. Klimas
5633 S. McAlees, Jr.
5633 R. E. Sheldahl
8266 E. A. Aas
DOE/TIC (25)
(R. P. Campbell, 3172-3)